OPTIMIZING ANALYTICAL METHODS FOR STUDYING MICROPLASTICS AND NANOPLASTICS AT THE MICROSCOPIC LEVEL

A Thesis

Presented to

The Faculty of the Department of Chemistry and Biochemistry California State University, Los Angeles

In Partial Fulfillment

of the Requirements for the Degree

Master of Science

in

Chemistry

By

Kevin Diego-Perez

December 2024

© 2024

Kevin Diego-Perez

ALL RIGHTS RESERVED

The thesis of Kevin Diego-Perez is approved.

Dr. Yixian Wang, Committee Chair

Dr. Linda Tunstad

Dr. Mathias Brieu

Dr. Petr Vozka

Dr. Krishna Foster, Department Chair

California State University, Los Angeles

December 2024

ABSTRACT

Optimizing Analytical Methods for studying Microplastics and Nano-plastics at the microscopic level

By

Kevin Diego-Perez

Plastics are indispensable in our daily lives, but their overproduction and inadequate disposal have made them harmful environmental pollutants. Despite their inherent durability, environmental factors like mechanical forces, temperature changes, and exposure to light can degrade plastics. This results in the formation of microplastics—particles smaller than 5 mm—which pose ingestion risks to wildlife, marine life, and ultimately, humans. These microplastics can go through further degradation that can change their properties and form nano-plastics that can potentially cause more harm. Our study concentrates on optimizing analytical techniques for studying these micro- and nano-plastics at microscopic level. We first fine-tuned scanning electron microscopy (SEM) and atomic force microscopy (AFM) for tracking the degradation of individual polyethylene terephthalate (PET) microplastics subjected to 45-days of UV exposure. The optimization of SEM was crucial due to microplastics' minute size and non-conductive properties, which can lead to image distortions. By employing low vacuum SEM, we bypassed the need for metallic coatings, eliminating potential artifacts caused by surface charging. Using Pinpoint AFM, we assessed individual PET microplastics at the nanoscale, yielding both topographical and mechanical insights, including data on the Young's modulus. Additionally, we explored the chemical changes of PET microplastics using attenuated total reflectance-Fourier Transform infrared (ATR-FTIR) spectroscopy. Through these

combined techniques, we discerned the physical, mechanical, and chemical alterations caused by UV induced Photo-oxidation. In the second subproject, we fabricated nano-plastics from commercial water bottles and tires using ball-milling, characterized their size, and used critical angle reflection imaging to investigate the absorption of heavy metal ions to these nano-plastics. This is the first time that the binding kinetics at nano-plastics were measured at the microscopic level.

ACKNOWLEDGMENTS

I would like to give my appreciation and thanks to Dr. Yixian Wang, for her continuous support and guidance in the end of my undergraduate and throughout my entire master's degree. I've caused her stress throughout the entirety of my master's program. Even so, her unwavering belief in my abilities has been a source of inspiration for me to pursue my dreams and commitments. I am also grateful to my committee members, Dr. Brieu, Dr. Tunstad, and Dr. Vozka, for their insightful feedback contributed to the success of my work. I'd also like to thank the Materials Characterization Laboratory (MCL), specifically Professor Patrick Hartunian and technician Amirhesam Shakibizadeh who trained me and supported me throughout my master's program. I'd also like to express my gratitude to Dr. Jiang for allowing me to use his instruments and lab for my experiments. I'd also like to express my thanks and gratitude to my lab members for their kind words of encouragement and willingness to help in my moments of stress, making my experience in the lab space unique and enjoyable. I would like to give my thanks specifically to Tony Tran, Kam Hang Chan, Christina Dhoj, Adaly Garcia and Isabel Garcia, for their guidance and support on both research and personal matters, which have been instrumental in helping me navigate the master's program. I'd also like to thank my parents for their unwavering support and encouragement throughout my entire academic journey. I'd like to also thank Dr. Fangyuan Tian and Ethan Lucsik for help in obtaining QCM data for my nano-plastic samples. Lastly, I'd like to thank the CREST Center for Advancement toward Sustainable Urban Systems (CATSUS) (HRD-2112554) for providing funding throughout my research and master's degree.

TABLE OF CONTENTS

Abstract iv

Acknowledgments vi

List of Figures ix

Chapter

1. Introduction 1

1.1 Plastic Pollution 1

1.2 Microplastics and nano-plastics 2

1.3 Scanning Electron Microscopy 6

1.4 Atomic Force Microscopy 7

1.5 Fourier Transform Infrared Spectroscopy 10

1.6 Nano-plastic Fabrication and Their Characterization 12

1.7 Critical Angle Reflection Imaging 14

1.8 Goal of Study 16

2. Experimental Details 18

2.1 Chemicals and Materials 18

2.2 Scanning electron microcopy sample preparation for UV degradation 18

2.4 Atomic force microscopy sample preparation for UV degradation 19

2.3 Fourier transform infrared spectroscopy sample preparation for microplastics UV degradation 21

2.5 Preparation and characterization of Nano-plastics 21

3. Results and Discussion 24

3.1 Morphological characterization of individual polyethylene terephthalate

microplastics throughout the degradation process 24
3.2 Chemical characterization of bulk polyethylene terephthalate microplastics throughout the degradation process 27
3.3 Mechanical characterization of individual polyethylene terephthalate microplastics throughout the degradation process 34
3.4 Size and Concentration Determination of Polystyrene Butadiene and Polyethylene Terephthalate Nano-plastic 39
3.5 Kinetics studying of Copper Adsorption onto nano-plastic using Critical Angele Reflection imaging 40
4. Conclusion 43
4.1 Microplastics physical, chemical and mechanical Degradation 43
4.2 Nano-plastics characterization and Kinetic difference overview 44
References…….....46

LIST OF FIGURES

Figure

1. Schematic of Plastic Bottle Degradation: From Pollution to Microplastics Through Five Mechanisms 2

2. Primary Routes of PET Degradation and Their End Products 5

3. Schematic Representation of Atomic Force Microscopy (AFM) Pinpoint Mode: Interaction Stages and Force Curve Generation 7

4. Modes of Fourier Transform Infrared Spectroscopy: Transmission, Attenuated Total Reflectance, and Reflectance 10

5. Schematic of Planetary Ball Mill Setup: Rotation and Sample Processing in Jars …….....13

6. Schematic of the CARI Setup for Reflectivity Measurement of Nano-Plastics on Glass Coverslips.....15

7. Sample Preparation for SEM Analysis of PET Microplastics: UV Degradation Exposure at Various Time Intervals 18

8. Sample Preparation for AFM Analysis of PET Microplastics: UV Degradation Exposure at Specific Time Intervals 19

9. Sample Preparation Workflow for UV Degradation Testing of PET Microplastics…….....21

10. SEM Imaging of PET Microplastics: Comparative Analysis of Low Vacuum and High Vacuum Conditions with Gold Coating.....24

11. Correlative Imaging of PET Microplastics Degradation: 4K Digital Microscopy and SEM Analysis Over 45 Days of UV Exposure 25

12. FTIR Reflectance Spectra of PET Microplastics: Effects of UV Exposure Over Time and Normalization Analysis 27
13. Analysis of Experimental and Literature Intensity Variations in the 690–1050 cm^{-1} Infrared Region 29
14. Comparative Study of Experimental and Literature Intensity Variations in Mid-Infrared Regions.....31
15. Comparative Analysis of Experimental and Literature Intensity Variations Across Key Infrared Regions.....32
16. Pre-Degradation Characterization of PET Microplastics: Optical Imaging and AFM Analysis of Morphology and Mechanical Properties.....34
17. Multimodal Analysis of PET Microplastics After 15 Days of Degradation: Optical Imaging, AFM, and Mechanical Property Mapping. 35
18. Optical and Mechanical Characterization of PET Microplastics: Effects of UV Exposure on Morphology and Young's Modulus.....37
19. Digital Microscope Imaging and Size Distribution Analysis of Polystyrene Butadiene Rubber and Polyethylene Terephthalate Microplastics by DLS.....39
20. Adsorption Kinetics of Copper Ions on Tire Nano-Plastics: CARI Imaging, Kinetic Fitting, and Equilibrium Dissociation Constant Analysis.....40
21. Adsorption Kinetics of Copper Ions on PET Nano-Plastics: CARI Imaging, Kinetic Fitting, and Equilibrium Dissociation Constant Analysis.....41

CHAPTER 1

1.1 Plastic Pollution

The discovery of Bakelite in 1907 marked the inception of plastics and the mass commercialization of synthetic and semisynthetic polymers.[1] Plastics and polymers are intrinsically interconnected, with polymers consisting of large molecular chains made up of repeating structural units called monomers.[2] Plastics, whether synthetic or semi-synthetic, are primarily composed of polymers. Both are broadly classified into three major categories: thermoplastics, thermosets, and elastomers, each distinguished by their unique properties.[3] Thermoplastics are characterized by their ability to be deformed and extruded upon heating, featuring linear or slightly branched polymer chains.[3] In contrast, thermosets undergo irreversible hardening upon curing and cannot be remelted or reshaped due to their tightly cross-linked polymer network.[3] Elastomers, on the other hand, are formed from lightly crosslinked structures, granting them their elastic nature.[3] The distinct properties of plastic polymers arise from their molecular arrangement and chemical characteristics, making them uniquely suited for specific applications.[3] Polymers' low cost, lightweight nature, and corrosion resistance have made plastics ideal substitutes for materials like silk and metals in various applications, thereby establishing plastics as essential commodities.[4]

There has been significant interest in plastic materials due to their continued production and increased rate of disposal.[4] Plastics contribute to 12% of municipal waste in the United States and their many derivatives have become hazardous pollutants.[4,5] Single-use plastics contribute 50% of all produced plastics and are typically discarded within a year of production.[5] Plastics inherently have a long lifespan and can persist in the environment between 20 and 500 years before decomposing.[6] Plastic decomposition is

dependent on several environmental factors. A significant contributor of plastic and material degradation is sunlight which for plastics can cause both photo-oxidative[7] and thermal degradation.[8] Plastic pollution is exacerbated by the mismanagement of plastic waste. It is estimated that 5 to 13 million tons of plastic enter the oceans every year.[9] The highest contributor of plastic pollution is polyethylene (PE) due its extensive use as one time use plastics and its derivatives such as low density and high density polyethylene.[10] Another significant pollutant is polystyrene (Styrofoam) due to its innate physical properties and low cost for packaging material.[11] Plastics such as Polyethylene terephthalate (PET) are extensively used in fabric material and every year 56 million metric tons are produced to make plastic bags, and plastic bottles.[12,13] However, during their lifetime, these plastics can become choking hazardous for aquatic life.[13] Efforts have increasingly focused on preventing further plastic pollution due to its detrimental effects on aquatic and terrestrial life.[12]

1.2 Microplastics and nano-plastics

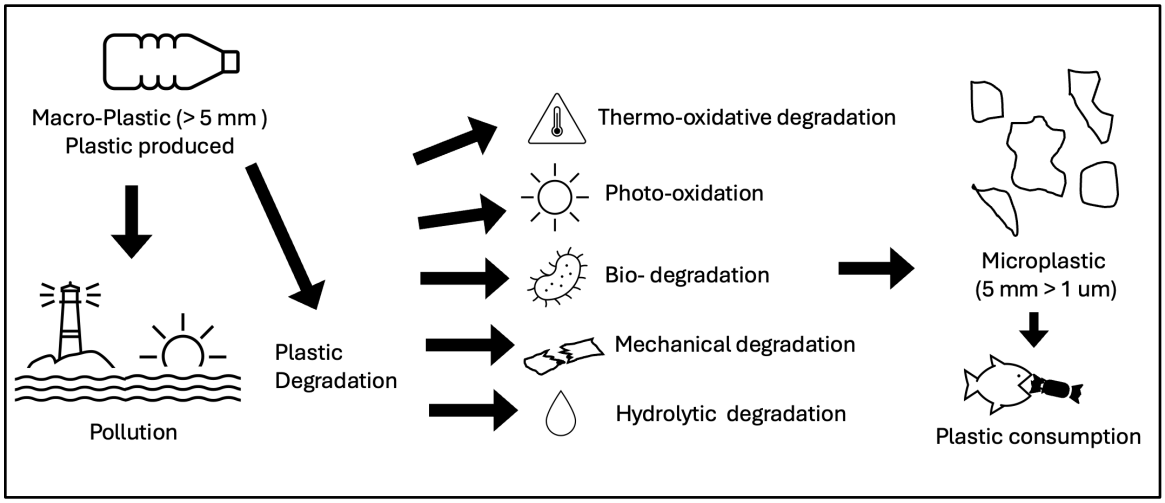


Figure 1. Schematic of plastic bottle becoming a pollutant and degrading into microplastics through 5 different mechanisms.

Microplastics (MPs) have become a significant focus of research due to their widespread environmental presence and potential impact on human health. Although MPs were first described in1970s, they were only recently termed “microplastics” by Richard Thompson OBE FRS in 2004.[14,15] MPs, defined as plastics particles ranging from 1 μm to 5 mm in size and classified into two groups: primary and secondary microplastics.[16] Primary MPs are commercially produced plastic particles commonly used for cosmetic products and industrial applications.[17] Secondary MPs result from the breakdown of larger plastics (Macro-plastics).[17] Although plastics degrade naturally over time plastics often take decades to degrade.[18] Environmental conditions and applications determine the rate of plastics degradation. For example, plastics can degrade via multiple different pathways such as hydrolytic,[8] thermo-oxidative,[17] photo-oxidative,[19] mechanical[20] and biodegradation.[11]

Secondary MPs and NPs are the most prevalent type of MP as they originate from several sources like artificial turfs, made from polypropylene and polyethylene.[21] Artificial turfs and infills are estimated to contribute 12% of plastic waste entering aquatic environments. Alternatively, Plastic based paints are also a significant contributor to MPs, as they eventually degrade and chip due to weather exposure. Car tires, wear away producing Rubber (Polystyrene butadiene) MPs that have been found distributed within and around roads.[22] Another significant source of MPs was Polyethylene terephthalate (PET), which contributes to 56 million tons of global plastic production annually.[12] PET is also extensively used in textile for polyester clothing a major source of Microfibril creation released during washing.[4,23] Increasingly studies have detected MPs in fish, salt, sugar,

food, and large bodies of water increasing heightened concern for chronic, low level ingestion.[24]

Research into MPs and NPs is crucial, as humans are estimated to consume between 39,000 to 52,000 plastic particles annually from various sources.[14] Although there is still speculation about the toxicity of MPs to humans their minute size poses a significant ingestion risk to mammals and aquatic life.[25] What is worrisome is MPs and NPs have been found in salts and drinking water likely leading to low exposure of MPs and NPs through ingestion.[26] MPs have been shown to cause intestinal blockages in fish and reduce fertility in some animals.[24] MPs have also been shown to move upwards through the food chain to humans.[16] Although larger MPs have been demonstrated in humans to travel passively through the gastrointestinal system. MPs have been known to mildly break down within the gastrointestinal system. This is concerning as MPs smaller than 2 μm has been noted to be internalized by human colon cells causing rearrangement of normal metabolic pathways. Exposure to NPs was also thought to have a role in the development of neurological disorders like Parkinson's.[27]

NPs are thought to pose a far greater threat to humans than MPs. Nano-plastic (size: 1 nm < 1 μm) can undergo translocation and can be taken up by cell inducing oxidative stresses.[28,29] NPs below 100 nm are able to translocate to every organ in the human body and pass the blood brain barrier.[30] MPs and NPs have been shown to be taken up by algae and microorganisms.[29] This is concerning because some aquatic life depend on algae and microorganisms to sustain themselves.[31] This has led to biomagnification within tropic levels.[31] More insight is needed into understanding MPs and NPs as the degradation processes changes innates properties of the material affecting adsorption properties.[31]

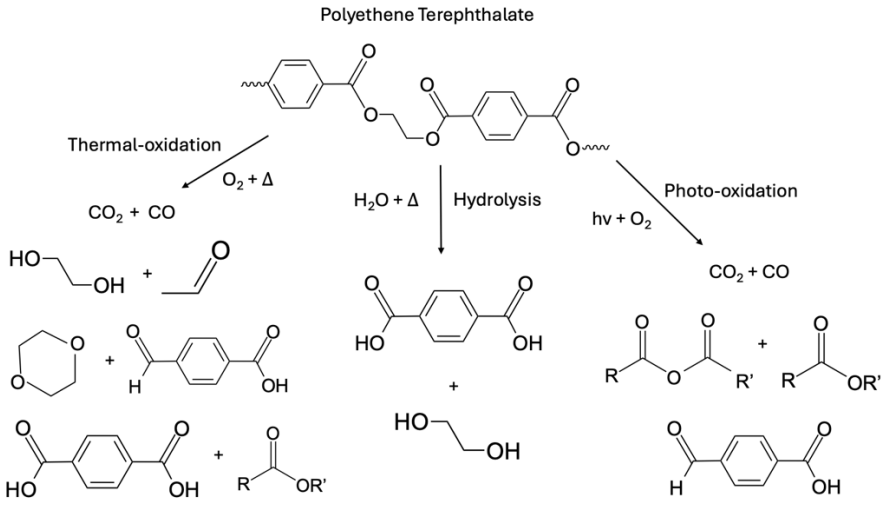


Figure 2. Primary routes of PET degradation and end products.

Single use plastics like PET will experience many forms of degradation such as photo-oxidation, thermal oxidation, and hydrolysis (Figure 2).[2] The prevailing mechanisms of degradation for PET is sunlight induced photooxidation.[3] The main step is chain scission which results in decreased molar mass and production of CO and CO_2.[3] Degradation via sunlight occurs in all plastics and is the main contributor to plastic and, in general, material degradation.[32] Degradation increases surface roughness and particularly via photooxidation has been found to produce surface reactive oxygen species and carboxyl end groups on the surface of MPs and NPs.[32] Degradation can change susceptibility of MPs and NPs becoming carriers for toxic chemicals.[17]

The coexistence of MPs and NPs with toxic materials has raised concerns about their role as transport vectors for harmful chemical compounds.[33] These compounds include heavy metals such as lead, copper, mercury and cobalt that have been linked to adverse health problems in humans.[34] The risks are exacerbated by degradation processes which alters both the chemical and physical properties of plastics, making the surface rougher and often times more absorbent.[35] The health risks imposed by MPs and NPs is

largely a consequence of their small size and large specific surface area.[36] Although, studies have shown that natural particles found in seawater are far more likely to adsorb heavy metal than MPs.[34] MPs and NPs are likely undergoing changes that impact adsorption properties such as surface moiety, crystallinity, surface charge, and specific surface area.[37] Microplastics (MPs) pose significant implications for human health, as they are continually generated not only in marine environments but also through daily human activities.[38]

Implication on human health is still a concern as MP and NPs are still an emerging area of study, and many techniques must be adapted to the field. There are also numerous plastics sources for MP and NP creation necessitating a threat assessment of MPs and NPs.[12] By standardizing methods to study MPs we can further extrapolate the risks imposed by MPs. Standardization of techniques will also ensure quality and consistency across MPs studies. Then to further NP research we have standardized a protocol for producing and characterizing the size and concentration of NPs. We then investigated the real time adsorption kinetic of NPs using critical angle reflectance (CARI) which has not been studied before.[27,31]

1.3 Scanning Electron Microscopy (SEM)

Scanning electron Microscopy (SEM) is a high-resolution imaging technique that can provide morphological information of a sample surface with nanometer resolution.[39] SEM utilizes electrons generated by an electron gun to produce an image. The electron beam produced follows a vertical path through the microscope, which is maintained under vacuum.[40] The Emitted electrons from the samples are detected by the detector enabling the creation of detailed images.[41] Often with nonconductive samples a thin conductive layer of metal is deposited on the sample for optimal scanning.[42] Alternatively, low vacuum

mode can be used, where the chamber is filled with water vapor to dissipate surface charges.[43] This can allow imaging of nonconductive samples without metal coating.[43] SEM can also be coupled with Energy dispersive X-Ray spectroscopy (EDS) to provide the elemental composition of the object by exciting atom at the samples surface.[44]

Here we report on using SEM to monitor the morphological changes of individual PET MPs that have undergone degradation for a span of 45 days. We optimized low Vacuum mode SEM to achieve high quality images without metal coating. This will allow us to track physical changes on the same MP. SEM will specifically be used to track changes in size, shape and surface morphology over a span of 45 days. Throughout this process we will set a standard protocol to prepare MPs for low vacuum SEM imaging.

1.4 Atomic Force Microscopy

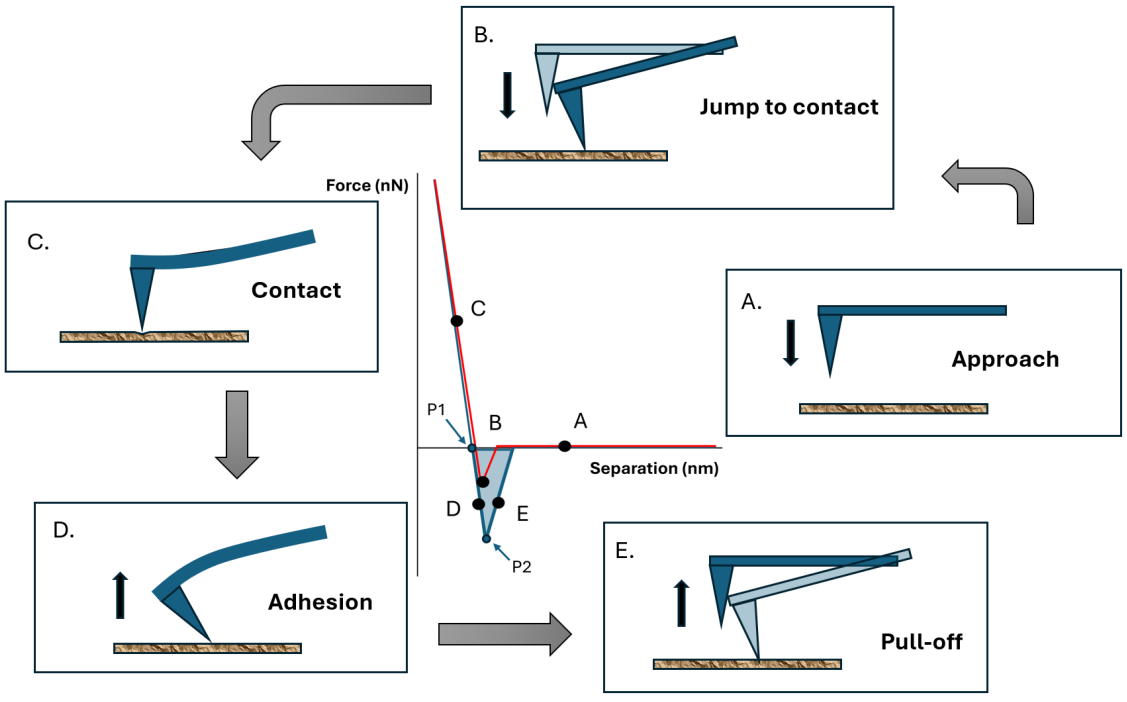


Figure 3. Schematic representation of atomic force microscopy (AFM) Pinpoint mode at a single point at different stages including the initial approaching the cantilever onto the sample surface **(A)**, intermolecular interaction causing the cantilever to be pulled to the surface **(B)**, cantilever in contact and impression into the sample **(C)**, the cantilever being

pulled off the sample and a lateral force adhesion preventing the cantilever from pulling off **(D)**, and finally the cantilever being pulled off **(E)**. The resulting force curve was plotted in the center.

Atomic Force Microscopy (AFM) is a scanning probe microscopic technique for surface characterization. Several AFM modes exist, including dynamic (tapping) mode, non-contact mode, and contact mode.[45] In AFM dynamic (tapping) mode, the cantilever oscillates perpendicularly to the surface as it scans, intermittently contacting the surface.[45] AFM non-contact mode involves the cantilever hovering above the sample surface, utilizing attractive and repulsive forces to measure surface characteristics without physical contact. AFM contact mode requires the cantilever tip to remain in continuous contact with the samples surface, to capture topographical data.[45] AFM Pinpoint is a derivative of AFM contact mode and in practice, single-point measurements are done where the tip indents the surface, employing contact mechanics to analyze these interactions.[46] Pinpoint mode measures nano-mechanical properties of samples by implementing force distance (FD) spectroscopy on the sample surface.[46]

AFM PinPoint mode represents a significant advancement in materials science by enabling the measurement of strength and elastic modulus in specific areas while also being able to assess changes in the adhesive properties of materials.[47] This improved method offers a more precise and detailed analysis to further enhance our understanding of material heterogeneity at the nanoscale level.[20] In recent years, there has been significant interest in the micro-scale analysis of material samples, particularly soft materials, due to their critical industrial applications.[20] Understanding the properties of soft materials is essential for developing new, advanced materials with unique characteristics such as self-healing, flexibility, and biocompatibility.[48] PinPoint mode is one of several nano-mechanical

measurement techniques used to characterize material properties. Other techniques include Peak Force Quantitative Nano-mechanical Mapping (Peak Force QNM) and Quantitative Imaging (QI, by JPK Instruments).[49] While these methods have been extensively used to probe the surfaces of cells, there are limited studies exploring the application of PinPoint mode on MPs.[20]

Mechanical properties such as the Young's modulus are intrinsic to materials, but they can change over time due to aging processes or degradation. Young modulus (denoted as E) and often referred to as the elastic Youngs modulus can be defined by the relationship of stress (σ) over strain (ε) and at low strain the relationship is linear ($E = \sigma/\varepsilon$).[20] The change in modulus can be caused by several factors including exposure to different temperatures and those listed in Figure 1.[50] Continuous exposure to mechanical stresses can lead to creep and eventual fractures, altering the Young's modulus.[50] AFM Pinpoint mode could allow for nanoscale investigation of degradation processes, such as those induced by UV exposure.[51] This technique can also provide insights into the material's heterogeneity, which is crucial for understanding material characteristics.[52] This is because materials durability and strength is correlated with the composition of trans and cis bonds within a material.[8] A material that contains more trans bonds is considered more crystalline and is often more brittle. While those with more cis bonds are amorphous and may be more flexible or softer. Oftentimes mechanical information such as this can obtained through universal testing machines which is not practical for nanoscale analysis of microscopic materials.[53]

$$E = \frac{3}{4}(1-v)^2\left(\frac{1-16^{1/3}}{3}\right)^{\frac{3}{2}}\frac{F_{min}}{(R(d_{zero}-d_{\min})^3)^{\frac{1}{2}}} \qquad (1)$$

These FD curves, as illustrated in Figure 3, provide detailed information on mechanical properties of the sample.[46] This is done by fitting the FD curves data to a theoretical equation to extract the Young's modulus. Here we used the Johnson–Kendall–Roberts (JKR) model. Where v = Poisson's ratio, R = tip radius, F_{min} = Minium Force to retract from the surface, d_{zero}= The point where the cantilever is neither pushed or pulled by intermolecular forces and $d_{\min}$ = the minimum distance where the cantilever is no longer being pulled in by adhesion.[54]

Using Pinpoint mode, we have quantitatively mapped and tracked the nano-mechanical changes caused by UV induced Photooxidation on PETm surface. Nano-mechanical characteristics of microplastics have not been readily studied and with our study we have looked at specific active aging sites on single PETm particles throughout 45 days of degradation. We have also set a standard protocol to prep and test microplastics using AFM Pinpoint mode.

1.5 Fourier Transform Infrared Spectroscopy

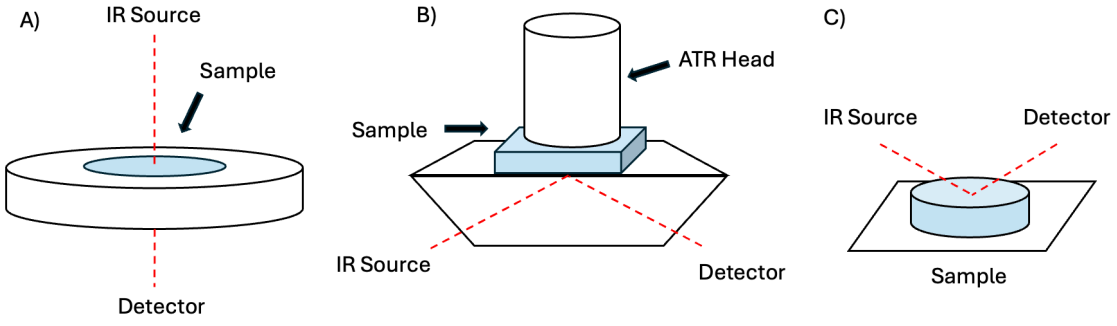


Figure 4. Modes of Fourier transform infrared spectroscopy including transmission (A), attenuated total reflectance (B), and reflectance (C).

Fourier transform infrared spectroscopy (FTIR) and derivatives of FTIR have been routinely used for the identification of unknown materials while being a nondestructive

technique.[55] In FTIR spectroscopy, an IR beam enters a Michelson interferometer, which splits the beam into multiple wavelengths.[56] These wavelengths are measured almost simultaneously by the detector, providing the chemical composition of the sample within minutes.[56] The IR beam is then introduced to the sample, either directly or through various methods.

In Transmission FTIR, the beam passes through the sample and into the detector.[57] In Reflectance FTIR, the beam reflects off the sample surface before reaching the detector.[58] Another common method is attenuated total reflectance (ATR) FTIR, where the beam enters an ATR crystal.[58] This crystal allows the beam to reflect multiple times off the sample before being detected. The detected wavelengths are subjected to Fourier transformation, resulting in a spectrum that identifies the sample's functional groups.[58] Identifying these functional groups is crucial as it helps determine polymeric changes caused by degradation. FTIR has become an essential tool to identify plastics polymers found in the environment. Understanding polymeric material chemical composition is important in both assessing longevity and performance of a polymers. Many studies have been able to use FTIR to track the UV degradation of plastics thin film such as Polyethene terephthalate (PET), polycarbonate (PC), and polyamide (PA).[25]

Using FTIR we planned to scan individual microplastics with FTIR reflectance. However, due to the thickness of the microplastic particles there was a poor signal to noise ratio. This was because reflectance FTIR works best on flat and reflective surfaces such as thin films. Our sample, while small, is also spherical which led us to perform bulk sample analysis using ATR-FTIR. This was to provide comprehensive information on the general

properties, specifically the conformational changes brought on by UV degradation processes.

1.6 Nano-plastic fabrication and their characterization

As mentioned previously, NPs are a cause for concern since they have environmental and health implications. However, nano-plastics found in the environment arise from the degradation of microplastics (secondary nano-plastics) or can be produced from commercial sources through chemical synthesis or physical grinding (primary nano-plastics). Primary MP and NP are either made through bottom-up approach (chemical synthesis) or top-down approach (mechanical alteration).[59] Bottom-up approach includes chemical synthesis through emulsion and nanoprecipitation.[60] The main benefit of synthesizing NPs is that quantification of important traits such as concentration, size, chemical functionalization and content of additives.[60] This makes the use bottom-up approach much more useful in the scientific field and many studies have already implemented the use of polystyrene NPs with chemical modifications. However, the main drawback is cost and production of plastic waste. The number of Nano-plastic in the environment cannot been readily quantified. Quantifying and analyzing nano-plastics in the environment is still a quite difficult task since NPs are both difficult to detect and separate.

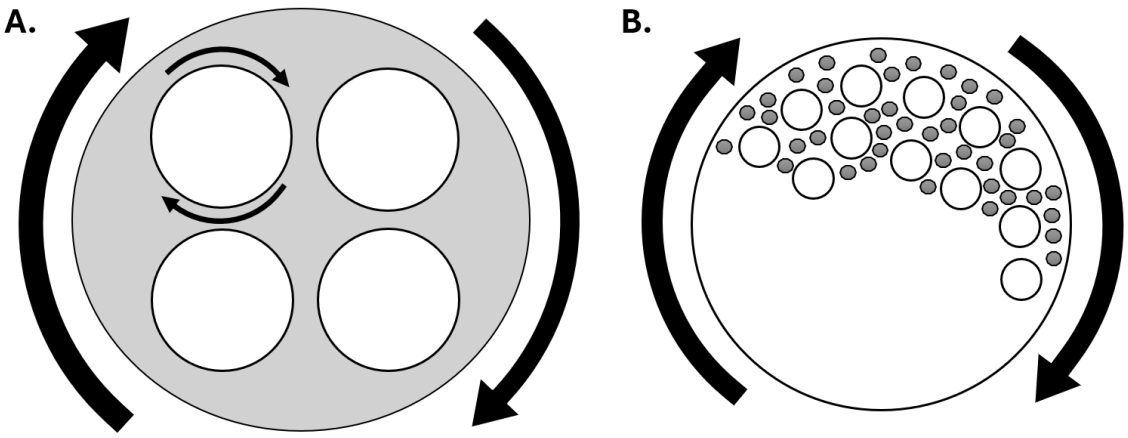


Figure 5. Schematic of planetary ball mill rotating clockwise with four jars (large white circles) (A) Simultaneously all four jars will spin clockwise filled with zirconia balls and a sample of choice (B)

Here, we use a top-down approach with a planetary ball mill to create nano-plastics, as ball milling is one of the most reliable methods for nanoparticle fabrication. Producing nano-plastics (NP) from existing plastic waste through ball milling is also beneficial. In ball milling, a rotating mill containing hard spheres (typically zirconia or steel) and the plastic sample is spun at high speed, causing collisions that grind the plastics down into micro- and nano-plastics. While nano-plastic formation occurs in the environment, the automotive recycling industry also uses milling techniques like ultra-centrifugal and ball milling for plastic waste processing.[60] Different milling procedures are used to obtain optimal sample size. Dry milling is used for materials that do not require a fine particle size and do not aggregate. In contrast, wet milling, which involves a solvent, prevents overheating, reduces particle aggregation, and avoids combustion of fine particles.

The main drawback to ball milling or top-down approach is the quantification of concentration and size of these particles. This requires the use of analytical techniques to quantify these properties. Dynamic Light Scattering (DLS) is a widely used technique to

determine the size of nanoparticles, typically in the nanometer range.[61] In this method, a laser is directed at a sample containing particles suspended in a solution.[61] The particles scatter the incident light, and their random motion—known as Brownian motion—causes fluctuations in the intensity of the scattered light.[61] These fluctuations are measured over time, and an autocorrelation function is used to analyze how the intensity changes. By correlating the light fluctuations with particle motion, the diffusion rate of the particles can be determined.[61] Using the Stokes-Einstein equation, this diffusion rate is then translated into an estimate of the particle's size, typically expressed as the hydrodynamic diameter.[61] This technique is particularly effective for measuring the size distribution of nanoparticles in suspension.

$$\Delta m = -C \cdot \frac{\Delta f}{n} \qquad (2)$$

Another technique used for measuring small quantities of material was Quartz Crystal Microbalance (QCM).[62] In QCM, an electric field is applied to a quartz crystal with electrodes attached to both sides, causing the crystal to vibrate at a specific resonant frequency.[62] The resonate frequency is innate and determined by the properties of the quartz. When a sample is applied to the surface of the crystal, the resonant frequency shifts.[62] This shift, denoted as Δf, can be correlated with the mass of the deposited material.[63] The overtone number (n) is related to the sample's material, while the mass sensitivity constant (C), depends on the properties of both the quartz and the sample. By measuring the frequency change (Δf), we can calculate the change in mass (Δm) and use QCM to determine the concentration of our in-house made nano-plastic solution.[63]

1.7 Critical Angle Reflection Imaging

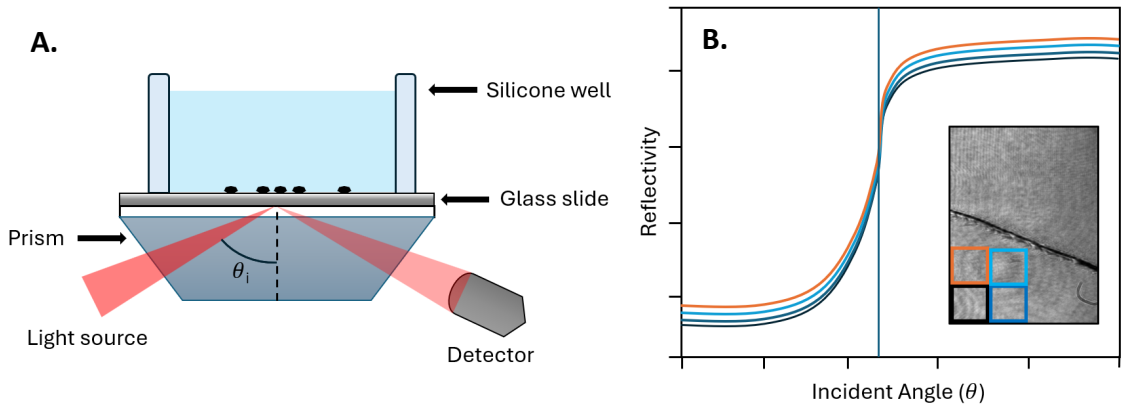


Figure 6. Schematic of the CARI setup. Nano-plastics on a glass coverslip placed on a prism-coupled imaging system with index-matching oil. The incident angle θ_i of a p-polarized light is set just below the critical angle (A). An angle sweep showing the reflectivity change as a function of incident angle at four regions of interest (ROIs) as labelled with color boxes in the inset CARI image (B). The blue solid line labels the selected incident angle for CARI.[64]

Critical Angle Reflection Imaging (CARI) is a newly developed imaging technique for monitoring molecular interaction and binding kinetics.[64] As shown in Figure 6A, the collimated incident light is reflected by the glass surface and a detection camera is focused at the sample layer on the surface to collect the reflected light.[64] The contrast of the image comes from reflectivity changes, which are modulated by the refractive index changes on or near the sensing surface.[64] The incident light is set at slightly below the critical angle to achieve an optimal sensitivity.[64] CARI has been approved capable of molecular interaction measurements including proteins, nucleic acid, and cell-based detections.[64]

In this study, we applied CARI to monitor the real-time adsorption of heavy metals onto NPs and analyze the kinetics of this process. While UV-Vis is a widely used technique for measuring metal adsorption, it requires isolating adsorbed metals before measurement, preventing real-time monitoring of interactions.[65] CARI addresses this limitation by

enabling continuous imaging, allowing for real-time analysis. Furthermore, CARI provides spatially resolved characterization, which can reveal sample heterogeneity.[64] We observed the binding kinetics of NPs from commodity plastics such as PET (from water bottles) and rubber NPs (from tires). CARI was used to observe copper adsorption with the two NP.

1.8 Goals of Study

Here we report on two subprojects that focus on setting protocols for plastics particles analysis at the microscopic level. The first focuses on optimizing three different analytical methods to characterize and quantify polyethylene terephthalate microplastics (PETm) degradation under UV exposure. Although extensive research has been conducted on the degradation of plastics into microplastics, few studies have explored the environmental impact of UV-degraded microplastics. Advancing research on this topic is essential to increase awareness of the potential hazards associated with degraded PET microplastics. We hope to reveal more information on the physical, mechanical, and chemical changes brought on by the degradation of PET microplastics under accelerated UV degradation. We will also set a standard protocol to analyze microplastics using spectroscopic and microscopic techniques. We will develop protocols to employ Fourier-transform infrared spectroscopy (FTIR), digital microscope Keyence VHX 7000 4K (DM), atomic force microscopy (AFM) and scanning electron microscopy (SEM) to facilitate the recurrent monitoring of the same microplastic particle.

The second is to fabricate nano-plastics from water bottles and car tires and investigate heavy metal adsorption to these nano-plastics. This research specifically seeks to inform on best practices for creating and characterizing nano-plastics. Using Critical angle reflectance imaging (CARI) we examined the chemical interaction of nano plastics

with copper. CARI will provide us insights into the potential absorption capacity of nano plastics in real time.

CHAPTER 2

Experimental Details

2.1 Chemicals and Materials

Copper (II) sulfate pentahydrate was purchased from Fisher Scientific (Waltham, MA). Polyethene terephthalate microplastics (PETm) were purchased from Nanochemazone (Alberta, CANADA). Light bulbs 4 Pack 25-Watt UV Light Bulb with Ozone (185nm/254nm) were purchased from Biamnocm. The UV chamber was constructed from cardboard and lined with aluminum foil. Conductive double-sided carbon tape (8 mm), glass slides, ethanol (100%), and Phosphate buffered saline (PBS) tablets were acquired from Fisher Scientific (Waltham, MA). Rubber nano-plastics were procured from discarded tires, and PET nano-plastics were fabricated from Arrowhead water bottles. All aqueous solutions were prepared with double-deionized water (resistivity = 18.2 MΩ·cm at 25 °C, Milli-Q Ultrapure water EQ 7000 Purification System, MilliporeSigma, Burlington, MA, United States). 4" diameter, Stainless Steel Frame/Stainless Steel Wire 0.33- and 1.0-mm sieves were purchased from Adamas Beta (Shanghai, China).

2.2 Scanning electron microcopy sample preparation for UV degradation

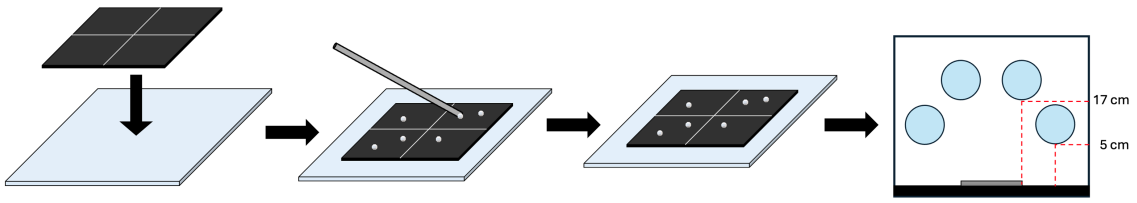


Figure 7. Sample preparation for microplastics UV degradation tests. PETm to be analyzed by SEM were placed on carbon tape fixed on a glass slide. Prepared microplastic samples were then placed into UV chamber for exposure of specific time intervals (0, 15, 30, and 45 days).

Three different sample preparations were used for optimal characterization with SEM, AFM and FTIR respectively. Nine individual PET microplastics were placed onto carbon tape attached to a glass slide (24 mm × 24 mm) for SEM characterization. Individual PETm were placed onto the carbon tape using clean Parr 45C10 fuse wire (34 B&S gauge), as shown in Figures 7. Prior to degradation samples were categorized with Digital microscope and SEM imaging. The particles were then introduced to the UV chamber, where the UV lights were kept on for 24 hours a day in 15-day increments. The chamber maintained an average temperature of 42.35 °C $\pm$ 1.69.

Samples were characterized before UV exposure and then after each 15-day UV exposure. Initial imaging was taken with Digital microscope Keyence VHX 7000 4K (DM) using full ring lighting for magnifications below 1000x and with depth composition feature for magnifications above 1000x. The area of particles was determined using Keyence software "measure tool" specifically the "polygon" feature. SEM imaging was then taken with Thermo-scientific AXIA^{TM} ChemiSEM^{TM} scanning electron microscope with Tungsten filament under low vacuum. For comparison, some samples were treated with a gold particle coating (Cressington sputter coater 108 auto) and imaged under high vacuum (10^{-4} Pa).

2.3 Atomic force microscopy sample preparation for UV degradation

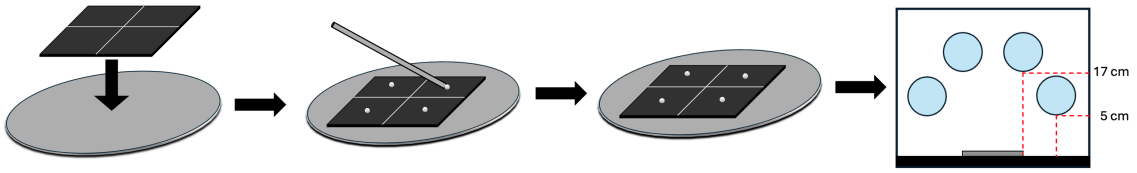


Figure 8. Sample preparation for microplastics UV degradation tests. Individual PETm to be analyzed by AFM were placed on carbon tape fixed on a magnet disk. Prepared microplastic samples were then placed into UV chamber for exposure of specific time intervals (0, 15, 30, and 45 days).

For AFM samples magnetic disk (diameter: 15 mm) substrate was used. Prior to degradation samples were categorized with AFM Pinpoint. The particles were then introduced to the UV chamber, where the UV lights were kept on for 24 hours a day in 15-day increments. The chamber, which was not temperature controlled, maintained a temperature between 42.35 °C $\pm$ 1.69. AFM samples were also imaged using Digital microscope Keyence VHX 7000 4K (DM) using the same parameter used for the SEM samples.

AFM samples were scanned using Park NX12 multifunctional microscopy platform equipped with a detachable AFM head (Park Systems, Seoul, South Korea). The instrument was operated with Smart Scan software (Park Systems, Seoul, South Korea). Nanomechanical studies were carried out through Pinpoint mode. AFM Contact cantilevers (OMCL-AC160TS, 26 N/m, 300 kHz) with a tip radius of 7 nm were used and were calibrated using the Sader method. We prepared 3 MPs that were each scanned 3 times (5.00 ×5.00 μm scans) 100 pixels in which the JKR model was applied. After degradation we were unable to do scans, so we instead opted to used single point analysis of several different location which were done in triplicate using the JKR model. From Pinpoint Mode we acquired AFM Z-height images which was 1st-order flattened with XEI (Park Systems, Seoul, South Korea). Flattening was performed to compensate for the slope and non-linearity introduced by the AFM piezoelectric scanner.

2.4 Fourier transform infrared spectroscopy sample preparation for UV degradation

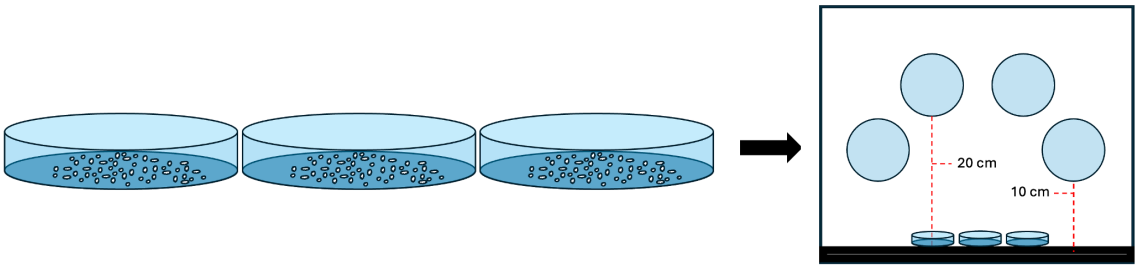


Figure 9. Sample preparation for microplastics UV degradation tests. Bulk sample was prepared by scattering PETm on a petri dish to be analyzed by FTIR. Prepared microplastic samples were then placed into UV chamber for exposure of specific time intervals (0, 15, 30, and 45 days).

FTIR analysis, samples were placed in 10.00 cm glass petri dish by covering the petri dish bottom with a thin layer of PETm particles. Prior to degradation samples the sample was categorized using FTIR-ATR. The particles were then introduced to the UV chamber, where the UV lights were kept on for 24 hours a day in 15-day increments. The chamber, which was not temperature controlled, maintained a temperature between 42.35 °C $\pm$ 1.69. The particles for FTIR analysis were shaken for approximately 30 seconds each day then placed back into the chamber to allow for homogeneous exposure. Chemical characterization was done with ATR-FTIR Microscope NicoletTM ContinuumTM in the range of 600–4000 cm^{-1} with 64 scans and data were processed in Excel.

2.5 Preparation and characterization of Nano-plastics

Nano-plastics were fabricated from PET bottles or tires. PET bottles were cut down to 1 cm and below and grinded down using a lejieyin grain mill (AZ, United States) for 10 minutes. Tires were cut using a handsaw for 1 hour to produce 6 grams of rubber particles. The resulting plastics particles from both materials were sieved separately through 0.33 mm and 1.00 mm sieve. Plastics above 1.00 mm were further grinded with lejieyin grain

mill. Only plastics from rubber and PET smaller than 1.00 mm were collected for ball-milling.

Ball-milling was conducted with PBM-04 Planetary ball mill (Brossard, Canada) that holds four Zirconia jars (100 mL each). An even number of jars must always be used, and each jar was filled a third of the way with zirconia balls. Particles between 0.33 mm and 1.00 mm were ball milled using 5.00 mm diameter zirconia balls to further reduce particles size. The resulting plastics were then combined with particles below 0.33 mm and further ball milled using 1.00 mm diameter zirconia balls.

Within each jar approximately 0.25 grams of plastics were milled at 450 RPM using unidirectional operation in nonfixed time mode for a period of 5 minutes and then allowed to cool at room temperature for 2 minutes. Ball-milling and cooling were repeated for a total of 9 cycles. The ball milled plastic particles were first sieved using 0.33 mm sieve, the resulting plastic particles were then sonicated for 20 minutes, and then filtered using a 1.00 μm syringe filter to only collect particles below 1.00 μm in size. The size distribution of both nano-plastic samples was obtained using dynamic light scattering (DLS) with a Malvern Zetasizer NanoS system (Malvern Panalytical, Westborough, MA). Nano-plastic concentration was approximated using Quartz crystal microbalance QCM200 – 5 MHz QCM, Standard Research Systems, (Sunnyvale, CA). Approximately 20 uL of the homemade solution was drop casted onto 25.4 mm QCM quartz crystal gold electrode. The frequency of the quartz chip was taken before and after the sample dried, we applied the Sauerbrey equation to the change in frequency.

For CARI tests, 5 μL of nano-plastics samples were drop-casted onto a clean glass cover slip then allowed to dry and then washed with distilled water and placed onto the

imaging platform. Copper solutions with concentrations of 10, 3.3, 1.1, 0.37, 0.122, and 0.041 mM were injected to the sample through a flow cell at a flow rate of 196 μL/min. CARI measurement was conducted using ImageSPR (Biosensing Instruments, Tempe, AZ) and the data was processed using ImageAnalysis (Biosensing Instruments, Tempe, AZ).

Chapter 3

Results and Discussion

3.1 Morphological characterization of polyethylene terephthalate microplastics

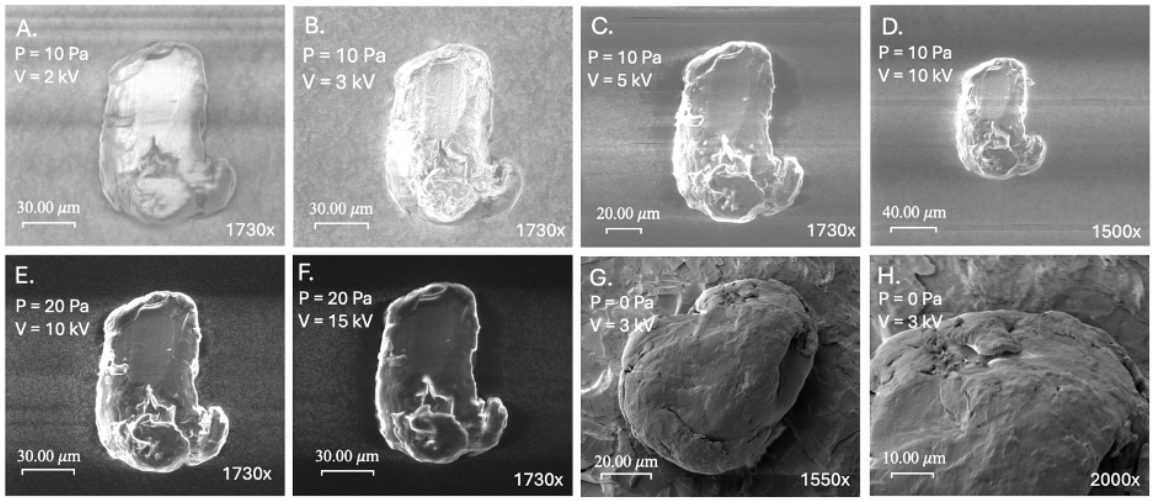
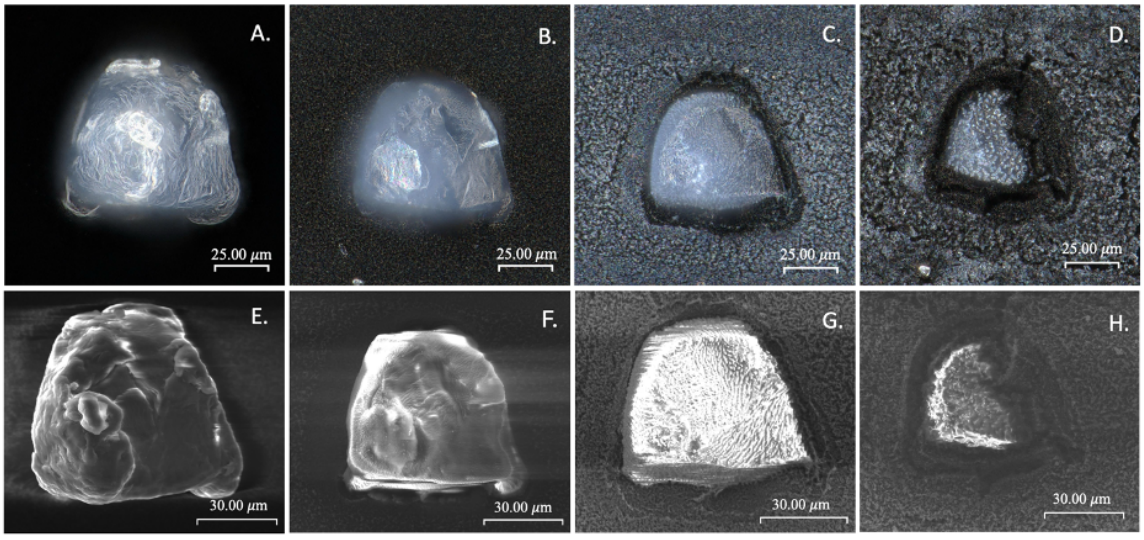


Figure 10. Scanning electron microscopy (SEM) imaging of a non-coated PETm particles under low vacuum mode at varying accelerating voltages (V) and pressures (P) (A-F) and a different PETm particle under high vacuum mode ($<10^{-4}$ Pa) sputtered coated with thin film of gold (G-H).

Immobilized PETm particles were tested under various pressures and accelerating voltages to optimize SEM imaging. Accelerating voltage is crucial because it determines the amount of energy with which the electrons impact the sample. Lower accelerating voltages are usually used with nonconductive materials whereas in high vacuum both low and high accelerating voltages can be used for conductive materials. Under high vacuum the chamber is ideally at a pressure of $< 10^{-4}$ Pa reducing. In low vacuum mode (LVM) SEM the pressure is above $< 10^{-4}$ Pa which allows for the introduction of water vapor which minimizes surface charging by dissipating the charge on nonconductive materials. Our goal was to achieve image quality comparable to Figures 10G and 10H without the use of gold coating. This choice was essential for our study, as gold coating would inhibit repeated monitoring of the same microplastic sample over the UV exposure period. Preliminary

results depicted in (Figure 10A-D) showed blurring at lower accelerating voltages but increased image sharpness at higher accelerating voltage but at the cost of surface charging near the edge of the particles. However, with LVM-SEM higher accelerating voltages are required to reach the sample due to the introduction of water vapor in the chamber. From Figure 10D to Figure 10E we compared the same accelerating voltages (10 kV) at higher pressures (20 Pa) this improved the image quality. Water particles are likely adhering more readily to the surface of PETm at higher pressures and dissipating the electrons at the surface reducing charging. We obtained similar results with 15 kV at the same pressures (20 Pa) but opted for lower voltage to minimize potential damage to the sample. Using LVM-SEM we can effectively image non-conductive materials by dissipating electrons away from the surface.



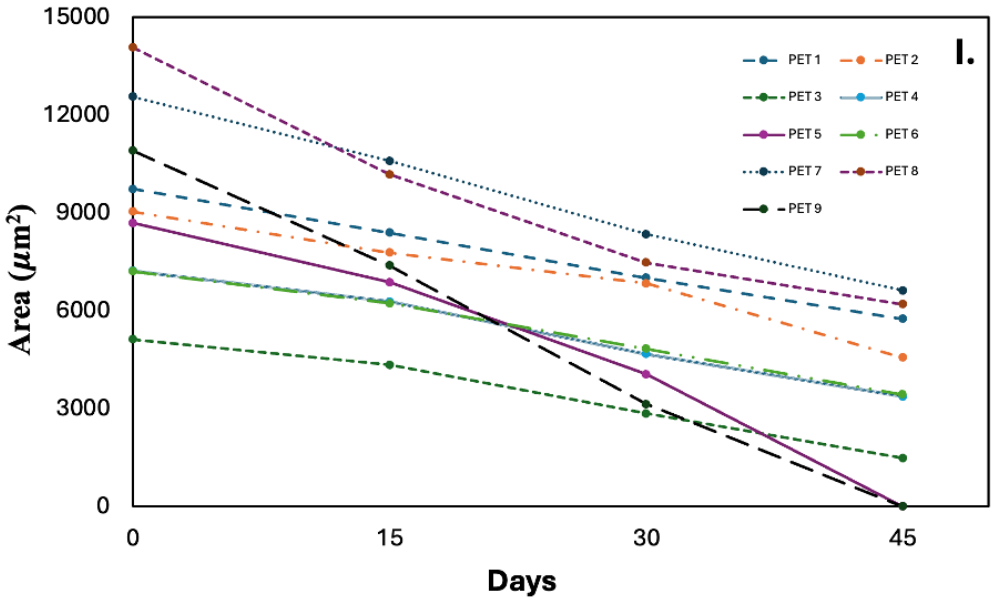
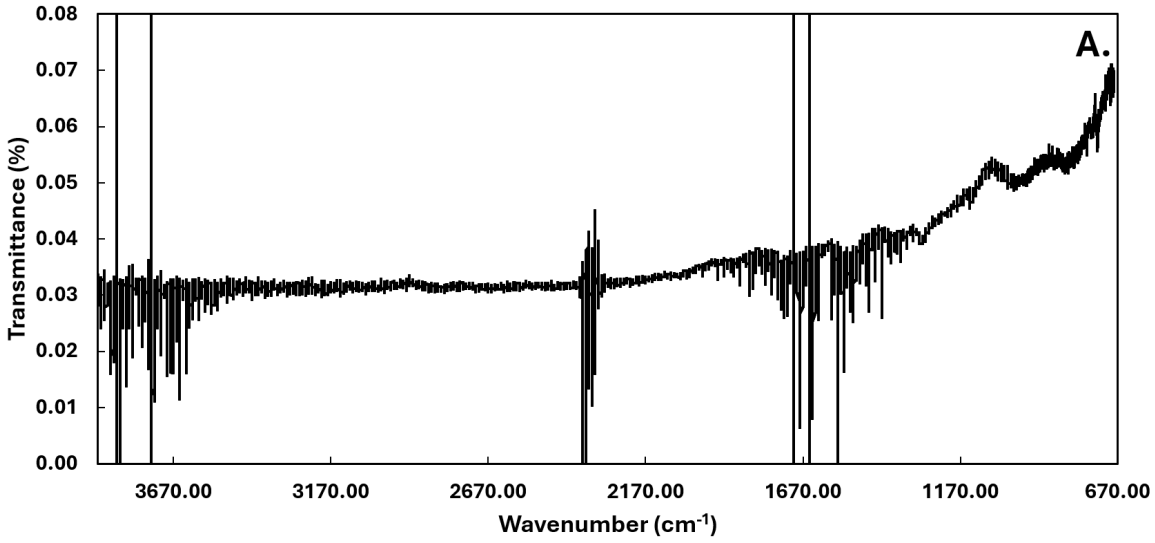


Figure 11. Keyence 4K Digital Microscope (DM) images **(A-D)** and SEM images **(F-H)** of the same PETm over 45 days of degradation. The images were collected with PETm before exposure **(A, E)**, after UV exposure of 15 days **(B, F)**, after UV exposure of 30 days **(C, G)**, and after UV exposure of 45 days **(D, H)**. Precise determination of the area from a top-down perspective of 9 different microplastics were determined using DM imaging **(I).**

We imaged nine different PET microplastic (PETm) samples using DM and SEM imaging over a span of 45 days. We used both tools as complementary techniques since SEM can provide finer image quality than that of DM imaging. DM imaging requires the use of "depth up" feature. "Depth up" compiles 200 images together from the lowest point to the highest point of a sample and stitches the 200 images together. Depth up feature may result in image blurring or glare that can be seen in figure 11B. In addition, only 200 images can be taken with this specific feature which may result in some details being lost but can be seen with SEM. For example, with DM imaging (Figure 11C) we see what looks like a smooth microplastics surface however with SEM (figure 11G) we can see what looks like the surface wrinkling. However, using both methods we can show the damage induced by UV radiation. Across 9 PETm samples there was an average reduced area of 37% after 45-days of UV exposure. The decreasing area of all 9 samples can be seen in Figure 11I.

SEM is often considered a destructive technique however we do not suspect that SEM is adding any additional damage to the sample since we see little to no change on the particle itself in Figure 10 even over an extended period of SEM imaging. However, to reduce possible chemical and mechanical changes caused by SEM we will use different samples for AFM and FTIR characterization. We do see that the carbon tape is undergoing degradation, which may affect AFM characterization although we believe carbon tape won't be ideal for long-term degradation studies we believe that for this study the carbon tape will be effective enough for 45 days. Alternative adhesives should be explored in future studies for longer degradation periods.

3.2 Chemical characterization of polyethylene terephthalate microplastics



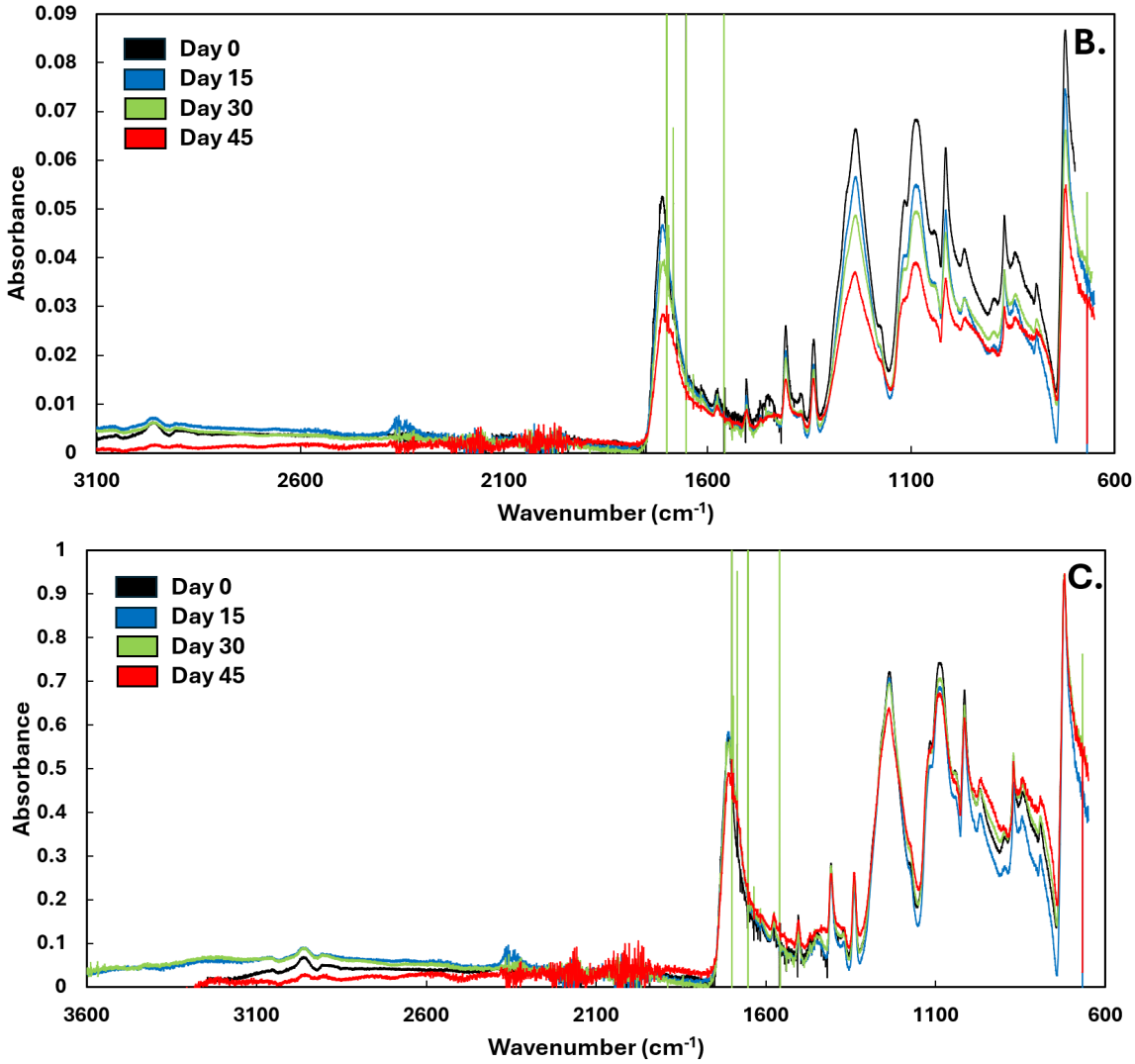


Figure 12. FTIR spectra of PETm using FTIR reflectance **(A)** Overlay of FTIR spectra of PETm under UV exposure for 0, 15, 30, and 45 days before **(B)** and after normalization with the peak at 723 cm-1 **(C)**.

To establish the baseline characteristics of polyethylene terephthalate microplastics (PETm), we performed reflectance FTIR characterization on bulk virgin MPs. Figure 12A depicts the graph obtained through FTIR Reflectance. We cannot see any apparent peaks of the polymer sample possibly due to low transparency of PETm particles. We moved from single particles analysis using reflectance FTIR to attenuated total reflectance FTIR (ATR-FTIR) which limited our analysis to bulk PETm particles.

Following baseline characterization of PETm using ATR-FTIR (Day 0), we subjected the bulk PETm particles to 45-days of degradation in 15-day increments. Figure 12B illustrates the raw ATR-FTIR scans of all peaks throughout 45-days of UV exposure. Overall absorbance of individual peaks decreased which in ATR-FTIR is commonly associated with a reduction in number of reflections with the sample, the decrease in number of molecules (decreasing size of the particles). Normalization was necessary to compare across different scans to account for these variations in peak intensity (height).

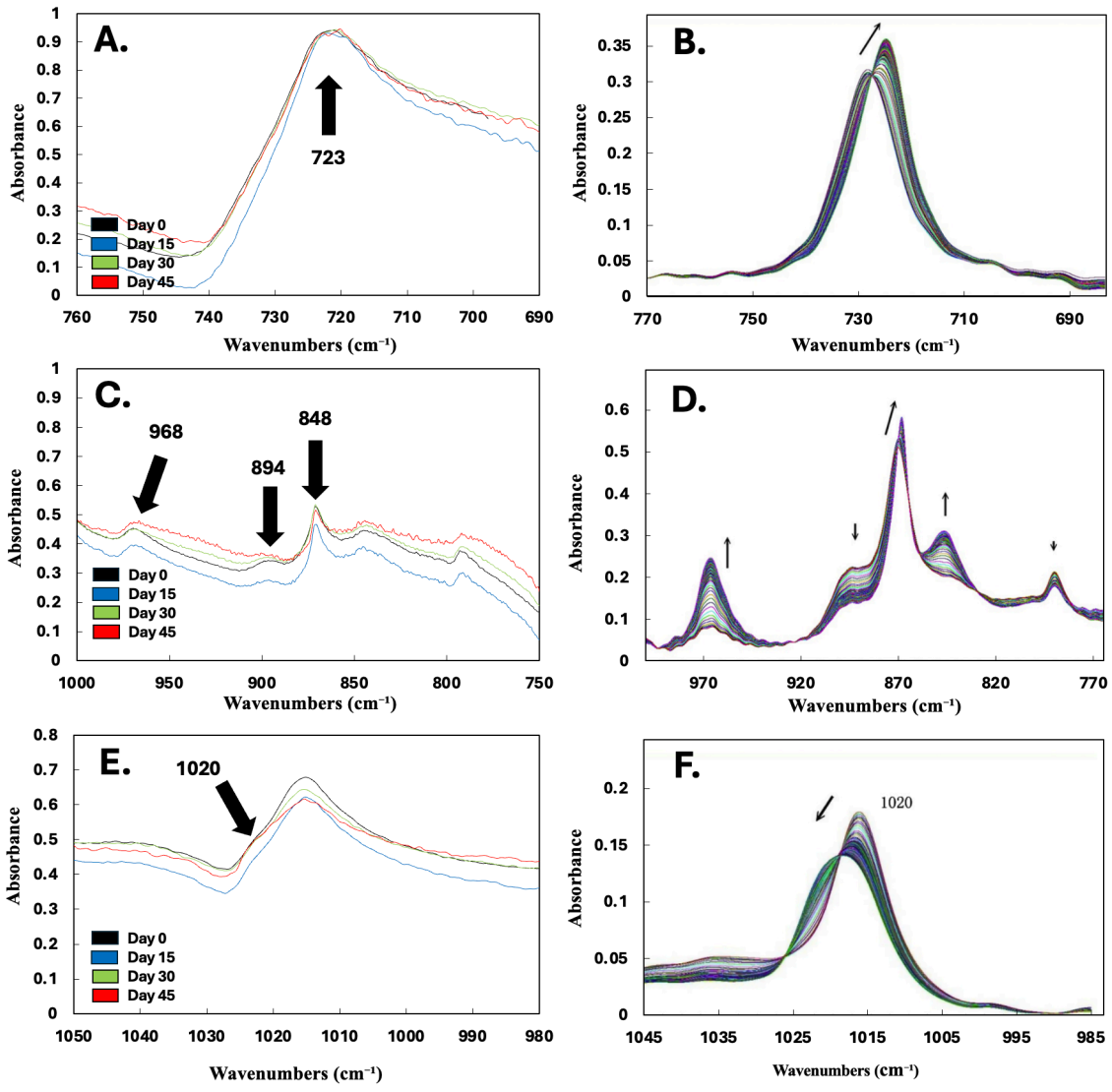


Figure 13. Experimental and literature intensity changes in the region 690 – 760 cm^{-1} **(A & B)**, 750 – 1000 cm^{-1} **(C&D)**, 1050 – 990 cm^{-1} **(E & F).**

Absorbance peaks were normalized to the 723 cm^{-1} peak (Figure 13C) which is associated with bending of the benzene ring. We compared our values on the left with those form literature which will be shown on the right (Figure 13B).[66] The literature focused on following PET conformational changes based on shifting FTIR peaks when PET is heated past its melting point and then allowed to cool.[66] In Figure 13B the shifting is the result of benzene ring bending from amorphous (cis isomer, 730 cm^{-1} region) to crystalline state (trans isomers, 723 cm^{-1} region). In our sample the absence of peak shift (the peak remaining in 723 cm^{-1} region) suggests that the benzene ring in the PETm particles was in the crystalline phase throughout the entire degradation process making it useful for normalization after 45 days of degradation.

We can further extrapolate changes in conformation when comparing absorbance peaks with those discussed in literature.[66] The peaks at 968, 848 and 894 cm^{-1} have been attributed to the conformation ethylene glycol unit's specifically the stretching of the (–C–H bond). The peaks at 968 cm^{-1} and 848 cm^{-1} belong to the trans isomers and the peaks at 894 cm^{-1} is assigned to the cis isomer depicted in Figure 13C. The literature values (Figure 13D) assume intensity changes are associated with conformational changes brought on by heating. Whereas in our sample during UV exposure, we see that all three peaks are decreasing which could indicate the disappearance of the ethylene glycol unit. In our sample we also see the disappearance of two absorption bands at 1095 and 1120 cm^{-1} Shown in Figure 14A is attributed to the cis isomer (amorphous) the trans (crystalline). Figure 13E, which is also associated with the ethylene glycol segment shows a decreasing peak intensity 1010 to higher wavenumbers in 1025 region depicted by the arrow. Although

chain is likely breaking due to chain scission the ethylene glycol unit was becoming more crystalline due to UV exposure.

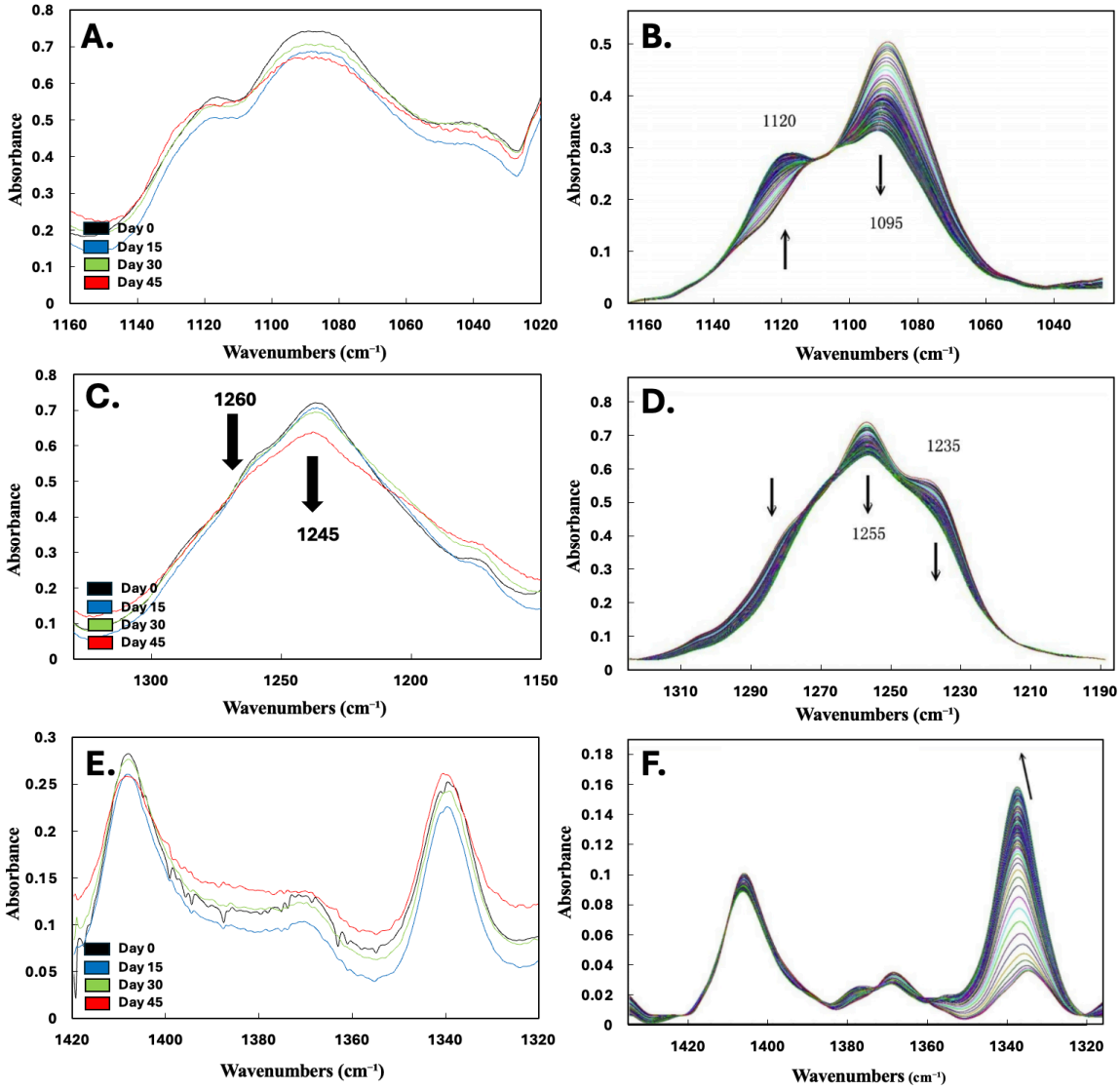


Figure 14. Experimental and literature intensity changes in the region 985 - 1050 cm^{-1} **(A & B),** 1050 – 1320 cm^{-1} **(D & C),** 1420 – 1320 cm^{-1} **(E & F)**.

We also encounter similar changes in peaks to those mentioned literature (Figure 10D) at 1235, 1255, 1285 and 1307 cm^{-1}. The 4 locations have been attributed to the stretching vibration of the ester group (–C–O–C=O) in its amorphous phase. Our scans showed decreasing band at all four regions (Figure 10C) and the resulting formation of one broad peak at the 1235 cm^{-1} region like the literature may imply that the ester group is

being incorporated into the crystalline region. The broadening of the peak insinuates that the PET microplastics are in fact becoming more crystalline within these specific regions.

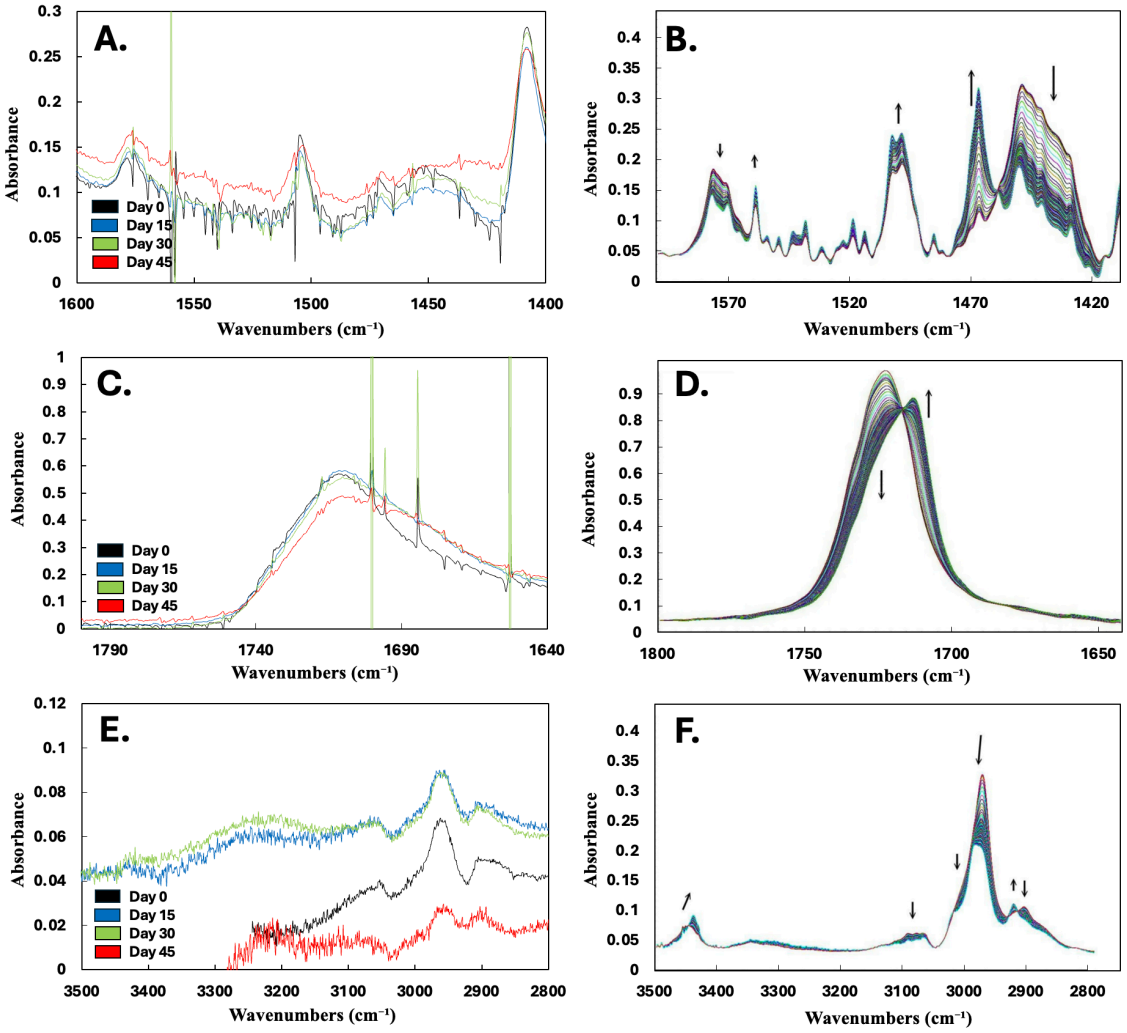


Figure 15. Experimental and literature intensity changes in the region 1400 – 1600 cm^{-1} **(A & B)**, 1800 – 1600 cm^{-1} **(C & D),** 3500 - 2800 cm^{-1} **(E & F).**

The peak found in the (1727 cm^{-1}) belongs to the carbonyl group (Figure 15A and 15B). The decreasing intensity and eventual developing peak at 1717 cm^{-1} (indicated by the arrows) is associated with the transition from amorphous to crystalline phase. The developing peak in 1717 region only begins to develop in day 45 but is another indicator of the gradual change in crystallinity of the polymer. The 3050 cm^{-1} regions can be

attributed to the four aromatic (C–H bonds) of the terephthalate ring while the peak at 2950 and 2910 cm^{-1} is associated with the aliphatic (–CH2–) groups (Figure 15E and 15F) in the ethylene glycol unit and in its cis conformation. The dropping intensity of both peak is a result of the phase transformation from cis to trans conformation (trans conformation being more crystalline). However as mentioned previously the peaks associated with ethylene glycol in other regions are also decreasing which may indicate the disappearance of ethylene glycol unit.

The literature attributes peak changes to conformational changes in the PET chain that make for a more crystalline polymer. What we assume is that the disappearing peaks are caused by UV induced photo-oxidation. This is likely causing chain scission in the ethylene glycol unit, leading to disappearing absorbance peaks in those regions. In addition, a more refined sample preparation for ATR-FTIR may be required as some specific regions such as those depicted Figure 14E and 15A seem to be affected by the granular shape of the particles. In these regions, peak variations prevent us from confidently assuming changes in the ethylene glycol unit.

3.3 Mechanical characterization of polyethene terephthalate microplastics

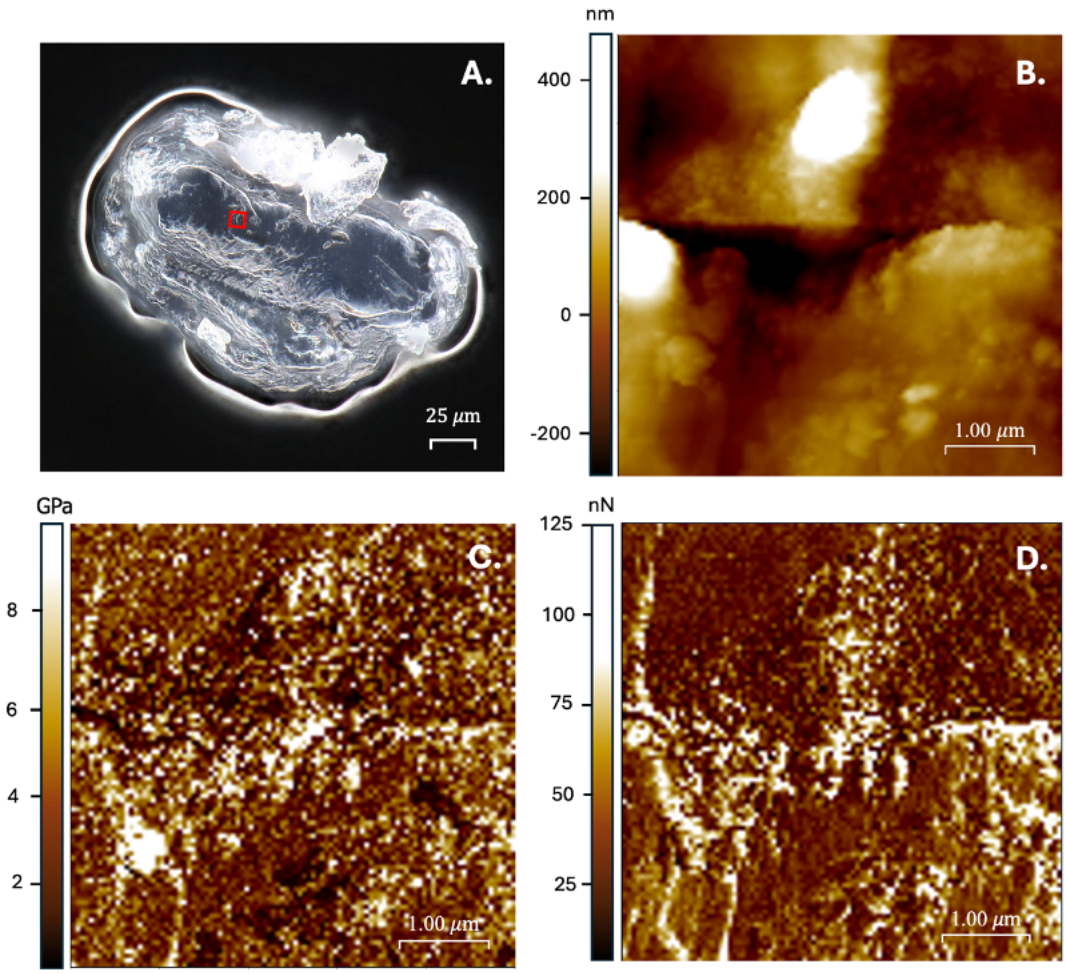


Figure 16. Optical image of a PETm before degradation at 1500× magnification. **(A)** AFM images **(B-D)** collected from the red box labeled in A with Pinpoint mode JKR, including height **(B)**, Young's Modulus **(C)**, and adhesion force **(D)**. Height was first ordered flattened.

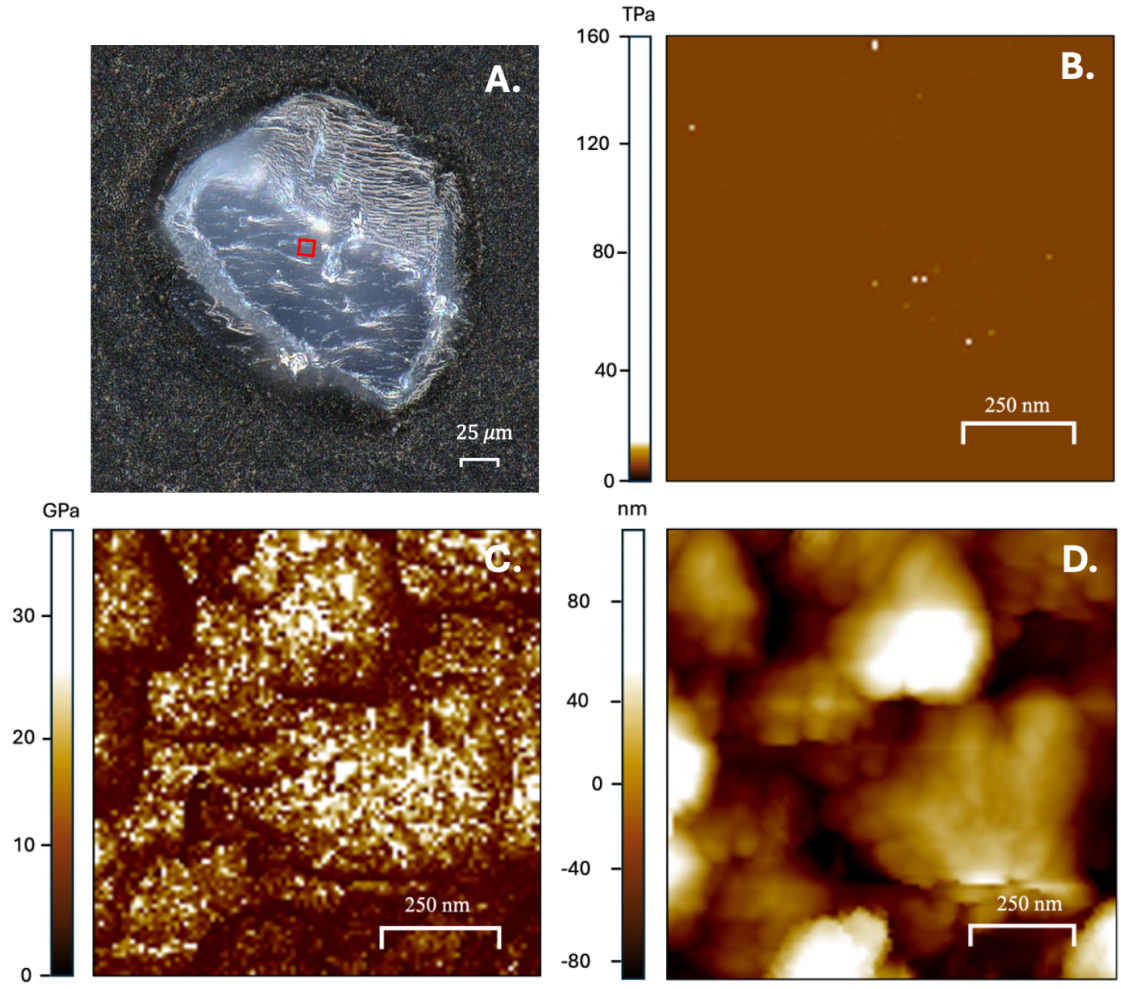


Figure 17. Optical image of a PETm after 15 days of degradation at 1500× magnification. **(A)** AFM images **(B-D)** collected from the red box labeled in A with Pinpoint mode JKR, including Young's Modulus with error **(B)**, Young's Modulus with errors removed **(C)**, and height **(D)**. Height was first ordered flattened.

The average reported Modulus for PET is 2.95 GPa. This is heavily dependent on how the sample is made since the modulus of PET can vary from 1.4 GPa to as high as 3.5 GPa. Using the JKR model on PET surface, we obtained a resulting Modulus of 3.154 GPa ± 0.512 (Figure 16). We found Pinpoint mode scanning with JKR after 15 days of UV exposure resulted in improper calculation of the Youngs modulus. Improper modulus calculation was apparent within a 5x5 um scan area since they appear as white dots and have a modulus of upwards of 100 Terra Pascals (Figure 16B). Realistically this is

impossible when you consider the average modulus of a diamond which is only 1200 GPa. We can sometimes attribute large jumps in modulus to noise that can be considered as outliers. But because there were changes to the samples surface due to aging several factors may affect Pinpoint mode scans. Differences in shape, size and roughness in the samples could result in improper calculations of the Youngs Modulus. This can include increased adhesion which necessitates a higher restoring force to separate the tip and sample thus giving an improper calculation. Presence of surface contaminants, changes in surface roughness, or changes in polymer heterogeneity.

To reduce improper calculations, we opted to preforms smaller 1x1 μm scans rather than 5x5 μm scans. The reduced size did not fix the error in calculations which is depicted in Figure 17B. The reduced size resulted in Modulus of 35.44 GPa $\pm$79.67. Errors such as these are not uncommon and could be caused by noise from outside forces. In which case XEI can be used to remove outliers caused by such noises (Fig 17C). After data processing the average Modulus was 9.5 GPa $\pm$ 3.916. However, the removal of these high modulus may not be ideal due to the level of manipulation required. Information result directly from degradation could have been removed. What is more concerning is that results across three different samples were all different using JKR.

Furthermore, interpreting Pinpoint mode data requires caution due to several influencing factors. During retraction, adhesion forces can induce a hysteresis effect, where the tip remains attached to the surface longer, necessitating a measurable force to detach. This phenomenon can impact results on a scan that composes of many pixels. In addition, Pinpoint mode initial approach is very important in obtaining a proper scan. Initial approach produces a force curve, as shown in Figure 3. Factors such as uneven surfaces

and varying intermolecular forces acting on the cantilever can also cause improper approaches, leading to errors in the calculation across several different force curves. Moreover, the compounding effect of each problem may result in the error of the modulus.

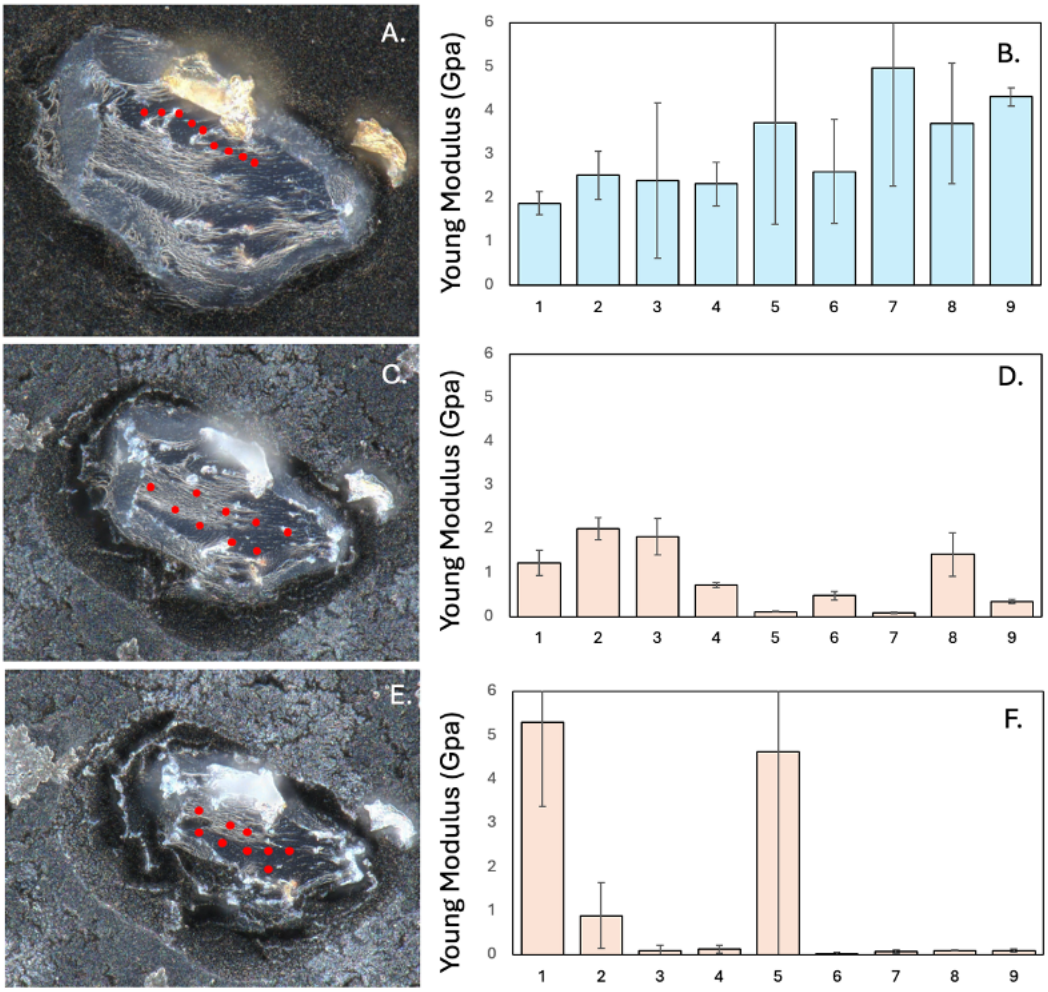


Figure 18. Optical images of the same PETm at 1500× magnification after UV exposure of 15 days **(A)**, 30 days **(C)** and 45 days **(E)** and the Young's Modulus collected from the nine spots labeled red in corresponding optical images **(B, D, F)**. Polyethylene Terephthalate (PET) microplastics (MP) (1500x). Young's moduli were extracted from F/D curve and ran in triplicates.

To avoid the above-mentioned problems and to cover as much sample surface as possible, we decided to only record force curves at individual spots dispersed over the whole microplastics rather than running scans on small areas. We observed that the

Young's modulus of the samples was decreasing. Although the Modulus stayed relatively the same over the first 15 days of UV exposure from 3.154 GPa ± 0.512 rose slightly to to an average 3.161 GPa ± 0.511 (figure 18A-B). After 30 days of exposure the Youngs modulus dropped to 1.266 GPa ± 3.076 then to 0.91 GPa ± 0.733 after 45-days of exposure.

The decreasing modulus indicates that the material was becoming softer with increased UV exposure. This was contrary to our expectations since we anticipated that the sample would become more brittle (higher Young's modulus).[66] This is also concerning because it is contradictory to our findings in FTIR data which insinuates that the sample was becoming more crystalline. We hypothesize that FTIR shows the overall change across the material whereas AFM-PM gives information uniformity of degradation across samples surface. This likely comes from the variations in the chemical composition and mechanical compositions at different layers within the same particle after UV degradation.[57] This could also be attributed to Photooxidation that may occurs more readily in the upper layers of the plastic rather than deeper layers which are deprived of oxygen.

However, the differences can also be the result of the transition from the hot UV-lit environment to room temperature. Although PET's glass transition temperature (69-89°C) and UV box only reaches temperatures of between 41°C and 43°C. The constant exposure to heat and then slow exposure to room temperature may be affecting the phase of crystallinity especially at the sample surface. The Youngs modulus of plastic are dependent on several mechanisms such as solidification after melting, nucleation, crystal growth from melting, and crystallization by stretching. For future experiments potential errors in AFM Pinpoint mode measurements cannot be completely ruled out. Since AFM

Pinpoint considers several factors when it comes to scanning samples. Even so AFM Pinpoint mode can map mechanical information at the surface with nanometer precision, allowing for detailed study of heterogeneous surfaces and materials.

3.4 Size and Concentration Determination of Polystyrene Butadiene and Polyethylene Terephthalate Nano-plastic

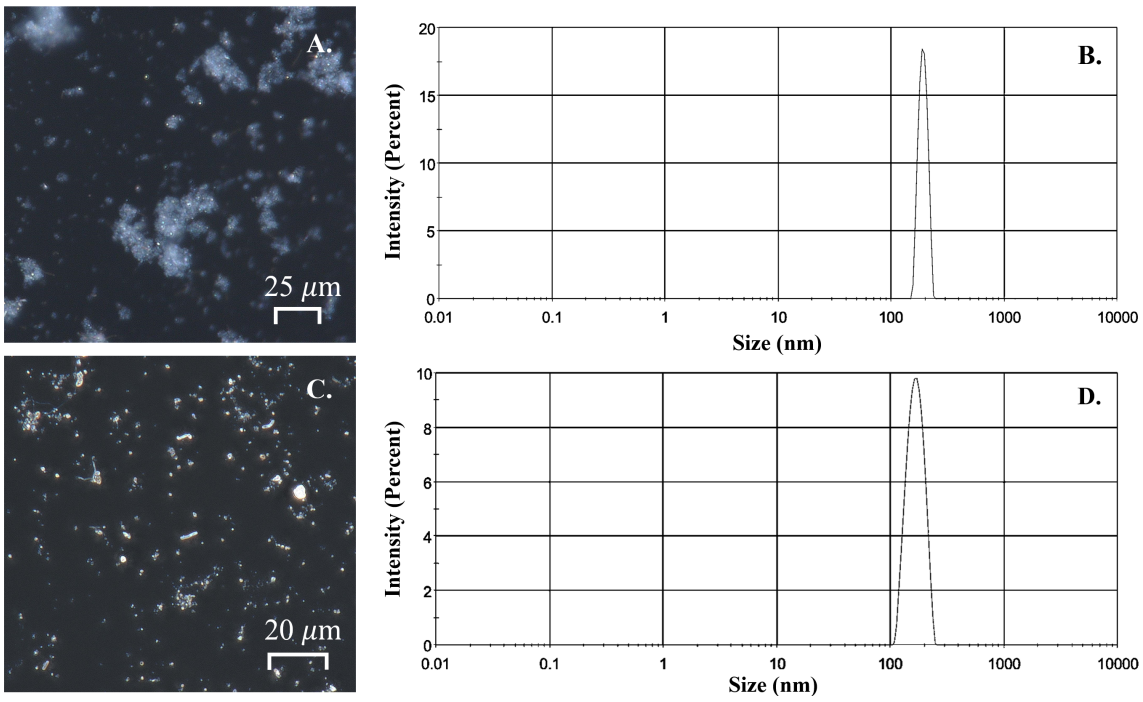


Figure 19. Digital Microscope (DM) of Polystyrene Butadiene (Rubber) **(A)** Size distribution plot of rubber nano-plastics obtained by Dynamic Light Scattering (DLS). **(B)** DM of Polyethylene terephthalate (PET) **(C)** Size distribution plot of PET microplastics obtained by DLS **(D)**

Using a refined literature-reported method for ball milling, we produced two distinct types of nano-plastics from polystyrene butadiene (Rubber) and water bottles (PET). Using QCM we were able to obtain the concertation of the ball milled solution. We obtained a concentration of 1.03 g/L ± 0.26 for rubber NPs and concentration of 0.41 g/L ± 0.32 for PET. Dynamic light scattering (DLS) was then used to determine the size distribution of nano-plastics prepared from Rubber and PET. Prior to analysis the bulk solution was sonicated for 15 minutes to prevent aggregation of the particles. The diameter

of the two nano-plastics samples were determined to be 195.50 ± 14.39 nm (rubber) and 229.20 ± 16.80 nm (PET).

3.5 Nano plastic Adsorption kinetics studying using Critical Angle Reflection imaging

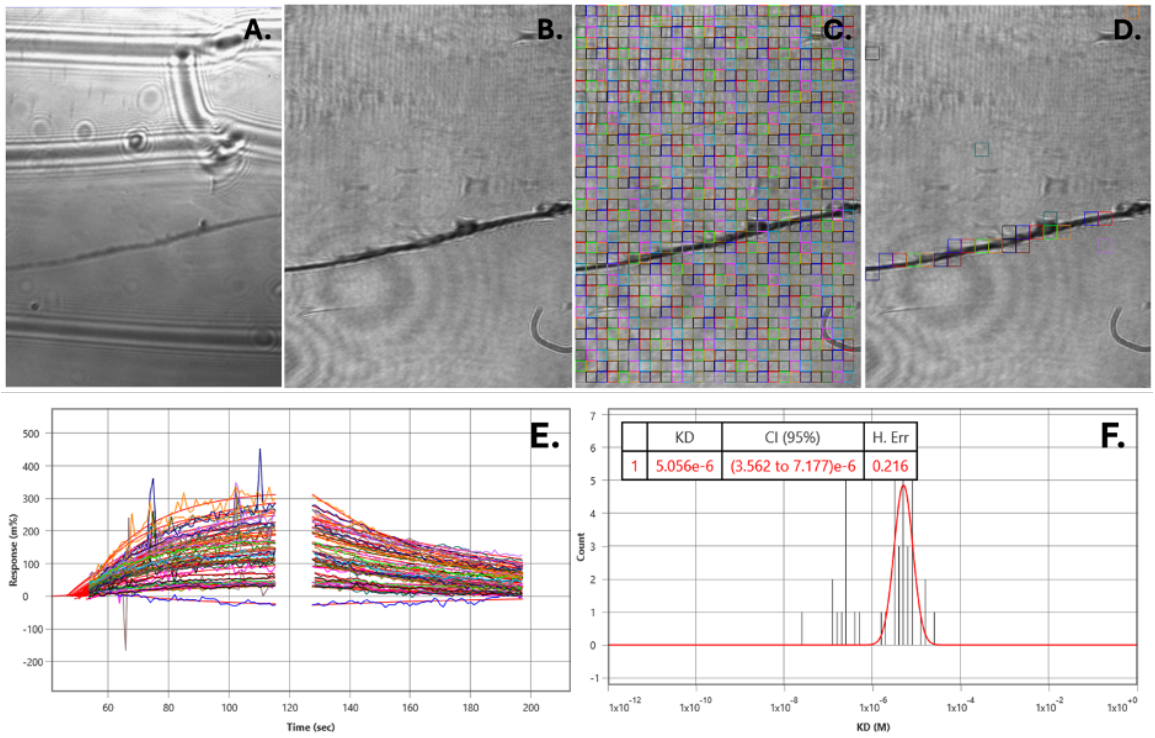
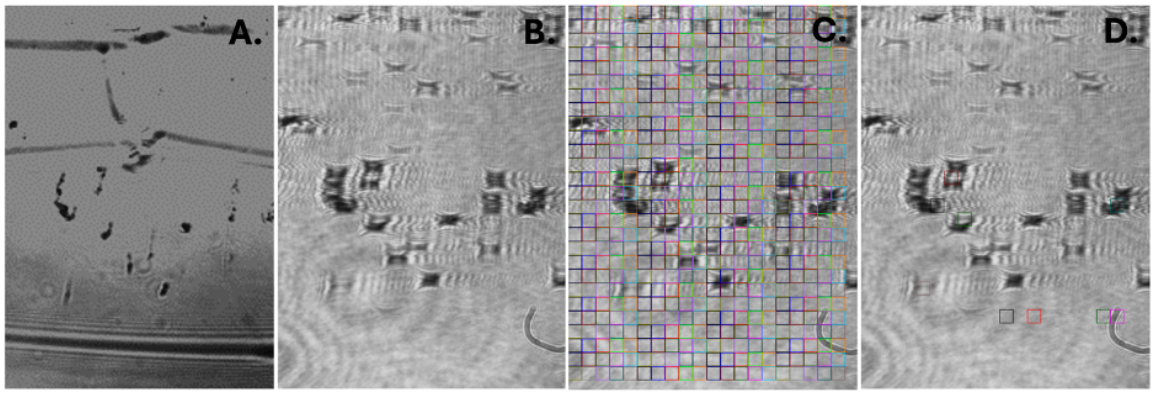


Figure 20. Representative results from CARI study of adsorption kinetics of copper ion to tire nano-plastics. Including the bright field image **(A)** and CARI images **(B-D)**, kinetic fitting of the association and dissociation curves **(E)** and the histogram of the resulting the equilibrium dissociation constant (KD) **(F)**. C shows the regions of interest (ROIs) enabled for kinetic analysis and D shows the remaining ROIs after filtering out the ROIs gave poor fitting. E and F only show the data from the remaining ROIs in D.



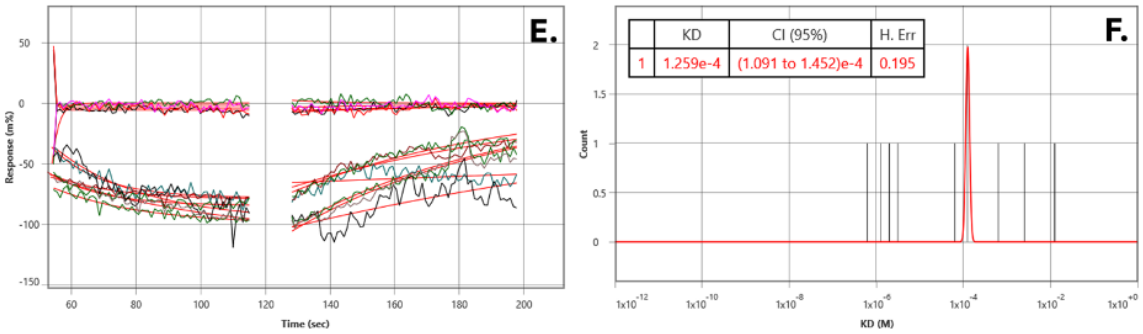


Figure 21. Representative results from CARI study of adsorption kinetics of copper ion to PET nano-plastics, Including the bright field image **(A)** and CARI images **(B-D)**, kinetic fitting of the association and dissociation curves **(E)** and the histogram of the resulting the equilibrium dissociation constant (KD) **(F)**. C shows the regions of interest (ROIs) enabled for kinetic analysis and D shows the remaining ROIs after filtering out the ROIs gave poor fitting. E and F only show the data from the remaining ROIs in D.

CARI allows us to study the adsorption kinetics of copper ion to nano-plastics. The tire nano-plastics sample showed typical association and dissociation of a first-order reaction at the plastic area, as shown in Figure 20. The following equations were used to run non-linear regression analyses on the experimental curves and to extract the kinetic parameters including association rate constant (k_a) and dissociation rate constant (k_d).

$$\frac{dR}{dt} = k_a C(R_{max} - R) - k_d R \quad (3)$$

$$\frac{dR}{dt} = -k_d R \quad (4)$$

Where R is the image intensity at individual ROI, *t* the time, C the concentration of copper, R_{max} the maximum concentration that can be adsorbed to the sample. Kinetics analysis was conducted for all ROIs shown in Figure 20C. After applying excluding filters related to fitting errors for k_a and k_d, only ROIs containing nano-plastics survived and gave an average KD (k_d /k_a) of 5.1 µM, with a 95% confidence interval of 3.6 - 7.2 µM

We didn't observe similar phenomena at PET nano-plastics. As shown in Figure 21, after the excluding filter applied, only six ROIs survived and distributed randomly with irregular association and dissociation profiles. There was no sufficient data to obtain the KD. However, it is safe to assume that copper ion shows a much slower and weaker adsorption to PET nano-plastics compared to tire nano-plastics. The rubber is an elastomer has lightly crosslinked polymer chains making it porous structure. Since it's a used tire various additives, fillers, and other chemicals still in the rubber nano plastics can interact with metal ions. Certain additives may have functional groups that form weak bonds with copper ions, facilitating absorption.

Chapters 4

Conclusion

4.1 Microplastic physical, chemical and mechanical Degradation

Our study investigated PETm exposed to UV light over a span of 45 days. We tracked the physical degradation using SEM and DM and were able to consistently show the decreasing size of 9 individual PETm plastics. DM imaging and SEM imaging were complementary techniques that allowed us to look both at the size and surface of the PETm. Although we found the optimal parameter for SEM-LVM there was still charging on the samples surface during SEM imaging which could be the result of the changing surface og individual PETm particle. Even aforementioned problems SEM and DM imaging can adequality show the physical changes as the result to UV exposure. Atomic force microscopy (AFM) Pinpoint was able to show the Young's modulus of the sample decreased over time. Decreasing Modulus indicates increased malleability and softness of the materials surface. Although we attribute the changing Modulus to UV exposure the high temperatures of 41°C and 43°C can be playing a factor. We mention this because it is contradictory to results found in FTIR which insinuates the polymer is becoming more crystalline. However, we must also keep in mind multiple factors that can result in errors of the Young's modulus such as the depth of UV degradation causing different layers to form in the same microplastics and different intermolecular forces on the surface. ATR-FTIR analysis was also adequately able to track conformal changes of PETm granules from UV exposure. Showing decreasing heights in certain region which is indicative of the transition from amorphous to crystalline phase in the PET chain while others were due to

chain scission. Using these optimized characterization techniques, we can track the degradation of PETm particles multiple characteristics.

4.2 Nano-plastic characterization and Kinetic difference overview

Synthesis of nano plastics through physical grinding was successful using the modified literature method. It allowed us to obtain polystyrene butadiene nano-plastics with an average size of 195 ± 14 nm. Using the same method, we were able to obtain PET nano-plastics with an average size 234 ± 168 nm. We were then the first to be able to adapt critical angle reflectance (CAR) to nano-plastics. Specifically, we were able test the kinetic interaction of PET and rubber nano plastics with copper. The interaction showed the adherence of copper onto rubber plastics but little to no interaction with PET nano-plastics. This is confirmed our suspicions since plastics such as PET are used primarily for water bottles and used readily for its inertness compared to other plastics. While rubber is an elastomer with more porous structure which gives rubber its innate flexibility than that of PET which contain a tightly linked structure.

With increased use of plastics, the creation of nano-plastics and Micro-plastics likely to occur. It is of utmost importance to adapt analytical methods into looking at morphological, chemical, and mechanical properties of microplastics. This is because ultimately Microplastics will become nano plastics. Nano plastics are especially concerning since they can be translocated throughout the human body and can become vector for heavy metal exposures. Because of this there is a need to understand the binding kinetics of nano plastics in real time which have become a ubiquitous contaminant in the environment. For future experiment will look at the adsorption kinetics of multiple heavy metals. In addition, a simplified kinetic model was used here to determine sorption rates.

Second-order and intraparticle diffusion are two model not applied here and will be considered for future experiments. We will also attempt to correlate the morphological/mechanical changes to the adsorption kinetics of both micro- and nano-plastics.

References

1. Issac, M. N.; Kandasubramanian, B. Effect of microplastics in water and aquatic systems. *Environ Sci Pollut Res* **2021***, 28*, 19544.

2. Chamas, A.; Moon, H.; Zheng, J.; Qiu, Y.; Tabassum, T.; Jang, J. H.; Abu-Omar, M.; Scott, S. L.; Suh, S. Degradation Rates of Plastics in the Environment. *ACS Sustainable Chem. Eng.* **2020***, 8*, 3494.

3. Liu, L.; Xu, M.; Ye, Y.; Zhang, B. On the degradation of (micro)plastics: Degradation methods, influencing factors, environmental impacts. *Science of The Total Environment* **2021***, 806*.

4. Browne, M. A.; Crump, P.; Niven, S. J.; Teuten, E.; Tonkin, A.; Galloway, T.; Thompson, R. Accumulation of Microplastic on Shorelines Woldwide: Sources and Sinks. *Environ. Sci. Technol.* **2011***, 45*, 9175.

5. Iroegbu, A. O. C.; Ray, S. S.; Mbarane, V.; Bordado, J. C.; Sardinha, J. P. Plastic Pollution: A Perspective on Matters Arising: Challenges and Opportunities. *ACS Omega* **2021***, 6*, 19343.

6. Delre, A.; Goudriaan, M.; Morales, V. H.; Vaksmaa, A.; Ndhlovu, R. T.; Baas, M.; Keijzer, E.; De Groot, T.; Zeghal, E.; Egger, M.; Röckmann, T.; Niemann, H. Plastic photodegradation under simulated marine conditions. *Marine Pollution Bulletin* **2023***, 187*.

7. Lin, J.; Yan, D.; Fu, J.; Chen, Y.; Ou, H. Ultraviolet-C and vacuum ultraviolet inducing surface degradation of microplastics. *Water Research* **2020***, 186*.

8. Miranda, M. N.; Sampaio, M. J.; Tavares, P. B.; Silva, A. M. T.; Pereira, M. F. R. Aging assessment of microplastics (LDPE, PET and uPVC) under urban environment stressors. *Science of The Total Environment* **2021***, 796*.

9. Ioakeimidis, C.; Fotopoulou, K. N.; Karapanagioti, H. K.; Geraga, M.; Zeri, C.; Papathanassiou, E.; Galgani, F.; Papatheodorou, G. The degradation potential of PET bottles in the marine environment: An ATR-FTIR based approach. *Sci Rep* **2016***, 6*.

10. Kühn, S.; Van Oyen, A.; Booth, A. M.; Meijboom, A. E.; Van Franeker, J. A. Marine microplastic: Preparation of relevant test materials for laboratory assessment of ecosystem impacts. *Chemosphere* **2018***, 213*, 103.

11. Yousif, E.; Haddad, R. Photodegradation and photostabilization of polymers, especially polystyrene: review.

12. Soong, Y. V.; Sobkowicz, M. J.; Xie, D. Recent Advances in Biological Recycling of Polyethylene Terephthalate (PET) Plastic Wastes. *Bioengineering* **2022***, 9*.

13. Sang, T.; Wallis, C. J.; Hill, G.; Britovsek, G. J. P. Polyethylene terephthalate degradation under natural and accelerated weathering conditions. *European Polymer Journal* **2020***, 136*.

14. Vasylius, M.; Tadžijevas, A.; Šapalas, D.; Kartašovas, V.; Janutėnienė, J.; Mažeika, P. Degradation of Mechanical Properties of A-PET Films after UV Aging. *Polymers* **2023***, 15*.

15. Zhu, L.; Xie, C.; Chen, L.; Dai, X.; Zhou, Y.; Pan, H.; Tian, K. Transport of microplastics in the body and interaction with biological barriers, and controlling of microplastics pollution. *Ecotoxicology and Environmental Safety* **2023***, 255*.

16. Alqahtani, S.; Alqahtani, S.; Saquib, Q.; Mohiddin, F. Toxicological impact of microplastics and nanoplastics on humans: understanding the mechanistic aspect of the interaction. *Front. Toxicol.* **2023***, 5*.

17. Tourinho, P. S.; Kočí, V.; Loureiro, S.; Van Gestel, C. A. M. Partitioning of chemical contaminants to microplastics: Sorption mechanisms, environmental distribution and effects on toxicity and bioaccumulation. *Environmental Pollution* **2019***, 252*, 1246.

18. Dimassi, S. N.; Hahladakis, J. N.; Yahia, M. N. D.; Ahmad, M. I.; Sayadi, S.; Al-Ghouti, M. A. Degradation-fragmentation of marine plastic waste and their environmental implications: A critical review. *Arabian Journal of Chemistry* **2022***, 15*.

19. Lee, C. O.; Chae, B.; Kim, S. B.; Jung, Y. M.; Lee, S. W. Two-dimensional correlation analysis study of the photo-degradation of poly(ethylene terephthalate) film. *Vibrational Spectroscopy* **2011***, 60*, 142.

20. Joshua, A. M.; Cheng, G.; Lau, E. V. Soft matter analysis via atomic force microscopy (AFM): A review. *Applied Surface Science Advances* **2023***, 17*.

21. De Haan, W. P.; Quintana, R.; Vilas, C.; Cózar, A.; Canals, M.; Uviedo, O.; Sanchez-Vidal, A. The dark side of artificial greening: Plastic turfs as widespread pollutants of aquatic environments. *Environmental Pollution* **2023***, 334*.

22. Kole, P. J.; Löhr, A. J.; Van Belleghem, F. G. A. J.; Ragas, A. M. J. Wear and Tear of Tyres: A Stealthy Source of Microplastics in the Environment. *IJERPH* **2017***, 14*.

23. Wang, W.; Wang, J. Comparative evaluation of sorption kinetics and isotherms of pyrene onto microplastics. *Chemosphere* **2017***, 193*, 567.

24. Yuan, Z.; Nag, R.; Cummins, E. Human health concerns regarding microplastics in the aquatic environment - From marine to food systems. *Science of The Total Environment* **2022***, 823*.

25. Ainali, N. M.; Bikiaris, D. N.; Lambropoulou, D. A. Physicochemical alterations on UV aged polymers leading to microplastics formation: A multi-tiered study of polyester, polycarbonate and polyamide. *Polymer Degradation and Stability* **2024***, 222*.

26. Wang, C.; Zhao, J.; Xing, B. Environmental source, fate, and toxicity of microplastics. *Journal of Hazardous Materials* **2020***, 407*.

27. Liu, Z.; Sokratian, A.; Duda, A. M.; Xu, E.; Stanhope, C.; Fu, A.; Strader, S.; Li, H.; Yuan, Y.; Bobay, B. G.; Sipe, J.; Bai, K.; Lundgaard, I.; Liu, N.; Hernandez, B.; Bowes Rickman, C.; Miller, S. E.; West, A. B. Anionic nanoplastic contaminants promote Parkinson's disease-associated α-synuclein aggregation.

28. Cox, K. D.; Covernton, G. A.; Davies, H. L.; Dower, J. F.; Juanes, F.; Dudas, S. E. Human Consumption of Microplastics. *Environ. Sci. Technol.* **2019***, 53*, 7068.

29. Neves, C. V.; Gaylarde, C. C.; Baptista Neto, J. A.; Vieira, K. S.; Pierri, B.; Waite, C. C. C.; Scott, D. C.; Da Fonseca, E. M. The transfer and resulting negative effects of nano- and micro-plastics through the aquatic trophic web—A discreet threat to human health. *Water Biology and Security* **2022***, 1*.

30. Zhang, Q.; Xu, E. G.; Li, J.; Chen, Q.; Ma, L.; Zeng, E. Y.; Shi, H. A Review of Microplastics in Table Salt, Drinking Water, and Air: Direct Human Exposure. *Environ. Sci. Technol.* **2020***, 54*, 3740.

31. Kalčíková, G. Beyond ingestion: Adhesion of microplastics to aquatic organisms. *Aquatic Toxicology* **2023***, 258*.

32. Prata, J. C.; Reis, V.; Paço, A.; Martins, P.; Cruz, A.; Da Costa, J. P.; Duarte, A. C.; Rocha-Santos, T. Effects of spatial and seasonal factors on the characteristics and carbonyl index of (micro)plastics in a sandy beach in Aveiro, Portugal. *Science of The Total Environment* **2019***, 709*.

33. Rai, P. K.; Sonne, C.; Brown, R. J. C.; Younis, S. A.; Kim, K. Adsorption of environmental contaminants on micro- and nano-scale plastic polymers and the influence of weathering processes on their adsorptive attributes. *Journal of Hazardous Materials* **2021***, 427*.

34. Chen, C. C.; Zhu, X.; Xu, H.; Chen, F.; Ma, J.; Pan, K. Copper Adsorption to Microplastics and Natural Particles in Seawater: A Comparison of Kinetics, Isotherms, and Bioavailability. *Environ. Sci. Technol.* **2021***, 55*, 13923.

35. Rowenczyk, L.; Dazzi, A.; Deniset-Besseau, A.; Beltran, V.; Goudounèche, D.; Wong-Wah-Chung, P.; Boyron, O.; George, M.; Fabre, P.; Roux, C.; Mingotaud, A. F.; Halle, A. T. Microstructure Characterization of Oceanic Polyethylene Debris. *Environ. Sci. Technol.* **2020***, 54*, 4102.

36. Turner, A. Paint particles in the marine environment: An overlooked component of microplastics. *Water Research X* **2021***, 12*.

37. Kinigopoulou, V.; Pashalidis, I.; Kalderis, D.; Anastopoulos, I. Microplastics as carriers of inorganic and organic contaminants in the environment: A review of recent progress. *Journal of Molecular Liquids* **2022***, 350*.

38. Kukkola, A.; Chetwynd, A. J.; Krause, S.; Lynch, I. Beyond microbeads: Examining the role of cosmetics in microplastic pollution and spotlighting unanswered questions. *Journal of Hazardous Materials* **2024***, 476*.

39. Wang, Z.; Wagner, J.; Ghosal, S.; Bedi, G.; Wall, S. SEM/EDS and optical microscopy analyses of microplastics in ocean trawl and fish guts. *Science of The Total Environment* **2017***, 603-604*, 616.

40. Fischer, E. R.; Hansen, B. T.; Nair, V.; Hoyt, F. H.; Dorward, D. W. Scanning Electron Microscopy. *CP Microbiology* **2013***, 25*.

41. Crawford, C. B.; Quinn, B. Microplastic identification techniques. In Elsevier: 2017; pp 219.

42. Sørensen, L.; Groven, A. S.; Hovsbakken, I. A.; Del Puerto, O.; Krause, D. F.; Sarno, A.; Booth, A. M. UV degradation of natural and synthetic microfibers causes fragmentation and release of polymer degradation products and chemical additives. *Science of The Total Environment* **2020***, 755*.

43. Kucheyev, S. O.; Toth, M.; Baumann, T. F.; Hamza, A. V.; Ilavsky, J.; Knowles, W. R.; Saw, C. K.; Thiel, B. L.; Tileli, V.; Van Buuren, T.; Wang, Y. M.; Willey, T. M. Structure of Low-Density Nanoporous Dielectrics Revealed by Low-Vacuum Electron Microscopy and Small-Angle X-ray Scattering. *Langmuir* **2006***, 23*, 353.

44. Zhang, W.; Dong, Z.; Zhu, L.; Hou, Y.; Qiu, Y. Direct Observation of the Release of Nanoplastics from Commercially Recycled Plastics with Correlative Raman Imaging and Scanning Electron Microscopy. *ACS Nano* **2020***, 14*, 7920.

45. Simpson, G. J.; Sedin, D. L.; Rowlen, K. L. Surface Roughness by Contact versus Tapping Mode Atomic Force Microscopy. *Langmuir* **1999***, 15*, 1429.

46. Garcia, R. Nanomechanical mapping of soft materials with the atomic force microscope: methods, theory and applications. *Chem. Soc. Rev.* **2020***, 49*, 5850.

47. Jariyavidyanont, K.; Yu, Q.; Petzold, A.; Thurn-Albrecht, T.; Glüge, R.; Altenbach, H.; Androsch, R. Young's modulus of the different crystalline phases of poly (l-lactic acid). *Journal of the Mechanical Behavior of Biomedical Materials* **2022***, 137*.

48. Akhatova, F.; Ishmukhametov, I.; Fakhrullina, G.; Fakhrullin, R. Nanomechanical Atomic Force Microscopy to Probe Cellular Microplastics Uptake and Distribution. *IJMS* **2022***, 23*.

49. Yablon, D. G.; Gannepalli, A.; Proksch, R.; Killgore, J.; Hurley, D. C.; Grabowski, J.; Tsou, A. H. Quantitative Viscoelastic Mapping of Polyolefin Blends with Contact Resonance Atomic Force Microscopy. *Macromolecules* **2012***, 45*, 4363.

50. Gulati, K.; Adachi, T. Profiling to Probing: Atomic force microscopy to characterize nano-engineered implants. *Acta Biomaterialia* **2023***, 170*, 15.

51. Ranjan, V. P.; Goel, S. Degradation of Low-Density Polyethylene Film Exposed to UV Radiation in Four Environments.

52. Chen, X.; Huang, W.; Tang, Y.; Zhang, R.; Lu, X.; Liu, Y.; Zhu, M.; Fan, X. Variation of Young's modulus suggested the main active sites for four different aging plastics at an early age time. *Journal of Hazardous Materials* **2024***, 470*.

53. Nair, S. S.; Wang, C.; Wynne, K. J. AFM Peakforce QNM mode for measurement of nanosurface mechanical properties of Pt-cured silicones. *Progress in Organic Coatings* **2018***, 126*, 119.

54. Prokopovich, P.; Perni, S. Comparison of JKR- and DMT-based multi-asperity adhesion model: Theory and experiment. *Colloids and Surfaces A: Physicochemical and Engineering Aspects* **2011***, 383*, 95.

55. Kühn, S.; Van Oyen, A.; Booth, A. M.; Meijboom, A. E.; Van Franeker, J. A. Marine microplastic: Preparation of relevant test materials for laboratory assessment of ecosystem impacts. *Chemosphere* **2018***, 213*, 103.

56. Othman, A. M.; Elsayed, A. A.; Sabry, Y. M.; Khalil, D.; Bourouina, T. Detection of Sub-20 μm Microplastic Particles by Attenuated Total Reflection Fourier Transform Infrared Spectroscopy and Comparison with Raman Spectroscopy. *ACS Omega* **2023***, 8*, 10335.

57. Fechine, G. J. M.; Rabello, M. S.; Souto Maior, R. M.; Catalani, L. H. Surface characterization of photodegraded poly(ethylene terephthalate). The effect of ultraviolet absorbers. *Polymer* **2004***, 45*, 2303.

58. Transform, F.; Spectroscopy, I.; Perkins The, W. D.; Corporation, P.; Avenue, C. chemical in/trument~tion Lexington. VA institute 24450.

59. Bruyère, D.; Simon, S.; Haas, H.; Conte, T.; Menad, N. Cryogenic ball milling: A key for elemental analysis of plastic-rich automotive shedder residue. *Powder Technology* **2016***, 294*, 454.

60. Lievens, S.; Vervoort, E.; Poma, G.; Covaci, A.; Van Der Borght, M. A Production and Fractionation Protocol for Polyvinyl Chloride Microplastics. *MPs* **2023***, 6*.

61. Falke, S.; Betzel, C. Dynamic Light Scattering (DLS). *Bioanalysis* **2019**, 173.

62. Rianjanu, A.; Fauzi, F.; Triyana, K.; Wasisto, H. S. Electrospun Nanofibers for Quartz Crystal Microbalance Gas Sensors: A Review. *ACS Appl. Nano Mater.* **2021***, 4*, 9957.

63. Alanazi, N.; Almutairi, M.; Alodhayb, A. N. A Review of Quartz Crystal Microbalance for Chemical and Biological Sensing Applications. *Sens Imaging* **2023***, 24*.

64. Ma, G.; Liang, R.; Wan, Z.; Wang, S. Critical angle reflection imaging for quantification of molecular interactions on glass surface. *Nat Commun* **2021***, 12*.

65. Cai, H.; Chen, M.; Du, F.; Matthews, S.; Shi, H. Separation and enrichment of nanoplastics in environmental water samples via ultracentrifugation. *Water Research* **2021***, 203*.

66. Chen, Z.; Hay, J. N.; Jenkins, M. J. FTIR spectroscopic analysis of poly(ethylene terephthalate) on crystallization. *European Polymer Journal* **2012***, 48*, 1586.